

AN EXTENSION OF THE APPROXIMATE COMPONENT MODE SYNTHESIS METHOD TO THE HETEROGENEOUS HELMHOLTZ EQUATION

ELENA GIAMMATTEO*, ALEXANDER HEINLEIN†, AND MATTHIAS SCHLOTTBOM‡

Abstract. In this work we propose and analyze an extension of the approximate component mode synthesis (ACMS) method to the heterogeneous Helmholtz equation. The ACMS method has originally been introduced by Hetmaniuk and Lehoucq as a multiscale method to solve elliptic partial differential equations. The ACMS method uses a domain decomposition to separate the numerical approximation by splitting the variational problem into two independent parts: local Helmholtz problems and a global interface problem. While the former are naturally local and decoupled such that they can be easily solved in parallel, the latter requires the construction of suitable local basis functions relying on local eigenmodes and suitable extensions. We carry out a full error analysis of this approach focusing on the case where the domain decomposition is kept fixed, but the number of eigenfunctions is increased. The theoretical results in this work are supported by numerical experiments verifying algebraic convergence for the method. In certain, practically relevant cases, even exponential convergence for the local Helmholtz problems can be achieved without oversampling.

Key words. Multiscale method, approximate component mode synthesis (ACMS), Helmholtz equation, heterogeneous media, high-frequency

AMS subject classifications. 65N12, 65N30, 65N35, 65N55

1. Introduction. In this paper, we propose and analyze a multiscale method for the heterogeneous Helmholtz equation

$$(1.1) \quad -\operatorname{div}(a\nabla u) - \kappa^2 u = f \quad \text{in } \Omega,$$

$$(1.2) \quad a\partial_n u - i\omega\beta u = g \quad \text{on } \Gamma_R,$$

$$(1.3) \quad u = 0 \quad \text{on } \Gamma_D,$$

in a plane region $\Omega \subset \mathbb{R}^2$. The boundary of Ω is decomposed into sets Γ_D and Γ_R modeling, respectively, Dirichlet boundary conditions and impedance boundary conditions described by the function g . The real-valued function β is related to transmission and reflection of the wave described by u . Material properties of the background medium occupying Ω are described by the coefficient functions a and c . Denoting the positive angular frequency as ω , the wavenumber is given by $\kappa = \omega/c$, and any interior sources are modeled by the function f . Heterogeneous Helmholtz equations have many applications, such as modeling the propagation of light in photonic crystals, where u is related to either the transverse-electric or the transverse-magnetic field [44], or seismic imaging [11, 57].

1.1. Literature overview. Numerical simulations of the Helmholtz equation are challenging due to the highly oscillatory behavior of the solution, in particular, in the case of a high wavenumber κ . The differential operator in the equation is indefinite, which may lead to stability issues for standard discretization approaches such as the classical finite element method (FEM). In order to resolve the oscillatory

*Department of Applied Mathematics, University of Twente, P.O. Box 217, 7500 AE Enschede, The Netherlands. e.giammatteo@utwente.nl

†Delft Institute of Applied Mathematics, Delft University of Technology, Mekelweg 4, 2628 CD Delft, The Netherlands. a.heinlein@tudelft.nl

‡Department of Applied Mathematics, University of Twente, P.O. Box 217, 7500 AE Enschede, The Netherlands. m.schlottbom@utwente.nl

behavior of the solution, a wavenumber-dependent mesh size of $\mathcal{O}(1/\kappa)$ is required. Moreover, the FEM solution suffers from the pollution error in general, i.e., the ratio of the errors of the Galerkin solution and the best approximation grows with the wavenumber κ [7, Theorem 2.6], [9]. To obtain accurate FEM solutions, a much smaller mesh size h satisfying $\kappa^3 h^2 = \mathcal{O}(1)$ has to be employed [22], see also [32, Theorem 4.5] where a similar condition is derived.

In order to overcome the pollution effect, higher-order methods can be employed: in particular, for the hp -FEM, quasi-optimality has been proved in [51, 52] under the conditions that the polynomial degree p is at least $\mathcal{O}(\log \kappa)$ and that $\kappa h/p$ is sufficiently small. In [16, 45], similar results have been achieved for the heterogeneous Helmholtz equation with piecewise smooth coefficients; however, to the authors' knowledge, no theory for rough coefficients is available yet.

Multiscale discretization approaches can be very efficient for problems with heterogeneous or non-smooth coefficients, especially if the variations are on a much smaller scale than the size of the computational domain. While for classical higher-order finite element methods, fine-scale coefficient variations have to be resolved by mesh elements, multiscale methods are typically defined on a coarser grid, and fine-scale variations are handled via adapted basis functions; those basis functions are typically computed locally using a fine-scale mesh. Hence, systems resulting from multiscale methods are often smaller by orders of magnitude.

In recent years, many multiscale discretization methods have been developed and applied to the heterogeneous Helmholtz equation; for a review on numerical homogenization techniques, also addressing their application to Helmholtz problems, see [4]. The localized orthogonal decomposition (LOD) method, introduced in [39, 50], has successfully been applied to heterogeneous Helmholtz problems with high wavenumbers [14, 54, 55]. The LOD relies on a partition of the domain with coarse elements of size H , and basis functions that are computed using local oversampling domains of size ℓH . The approximation error is then bounded by $\mathcal{O}(H + \gamma^\ell)$ for some $0 < \gamma < 1$ assuming the resolution condition $H\kappa \ll 1$ and $\log(\kappa)/\ell$ bounded [54, Theorem 5.5]. More recently, even super-exponential convergence of the localization error could be shown for a variant of the LOD method in [27].

The heterogeneous multiscale method (HMM) [2, 23], which relies on local periodicity of the media, has been extended to Helmholtz problems in [53]. The authors show quasi-optimality in terms of a wave-number dependent quasi-optimality constant.

Other multiscale discretization approaches are multiscale FEM (MsFEM) [6, 8, 42]; see also, e.g., [25] for an overview on MsFEM. Nearly exponential error decay has been achieved in [48], using similar ideas as in the multiscale generalized finite element method (Ms-GFEM), first described in [24]. In a recent work, Chen, Hou and Wang [18] extended ideas from elliptic equations [41, 17] to the heterogeneous Helmholtz equation. The method in [18] decomposes the solution into a microscale part, which is bounded by $\mathcal{O}(H)$, and macroscale part, which is bounded by $\mathcal{O}(H\gamma^m)$ for some $\gamma < 1$ and m denoting the number of local basis functions associated to the edges of a coarse partition with mesh size H . These local basis functions are computed by local oversampling.

In domain decomposition methods, multiscale discretizations are also used as coarse spaces to construct preconditioners which are robust with respect to heterogeneous coefficients; see, e.g., [1, 29, 37, 38] for applications to scalar elliptic problems, or [15] for linear elasticity problems. For the application to heterogeneous Helmholtz problems, see, for instance, [10, 19, 31].

Let us also refer to [57] for an optimized parallel implementation of a direct solver

based on local Schur complements on a hierarchy of domain decompositions reducing the number of low-rank compression operations compared with other structured direct solvers; see [47] for a recent work in the context of elliptic equations. Finally, multigrid methods for the heterogeneous Helmholtz problem have been analyzed; see, e.g., [26].

In this work, we consider an extension of the approximate component mode synthesis (ACMS) method to Helmholtz problems. The ACMS method has been introduced by Hetmaniuk and Lehoucq in [41] as a multiscale discretization for scalar elliptic problems with heterogeneous coefficient functions. It is based on the early component mode synthesis (CMS) method [21, 43], which uses a decomposition of the global approximation space into independent local subspaces and an interface space. The basis functions are defined as eigenmodes of corresponding generalized eigenvalue problems. The global support of the interface basis functions leads to high computational cost for their construction as well as a dense matrix structure of the interface problem. Hence, the practicability and potential for parallelization of CMS method are rather limited. Therefore, the ACMS method was introduced in order to improve the CMS approach: instead of global interface modes, functions with local support are employed. The basis functions incorporate heterogeneities of the model problem; notably, besides edge modes, this framework uses vertex basis functions of MsFEM [25, 42, 15] type. Since the ACMS discretization uses problem-specific shape functions with local support, it can therefore be considered a special finite element method (SFEM) [6], and it also fits into the framework of the generalized finite element method (GFEM) [5]. In contrast to other multiscale approaches, such as those previously mentioned [18, 27, 48], the ACMS method of [41] is based on a non-overlapping domain decomposition and does not use local oversampling.

The ACMS method has been further investigated in [40], where a priori error bounds and an a posteriori error indicator for the method have been derived, and in [35], where a parallel implementation in PETSc based on the finite element tearing and interconnecting dual primal (FETI-DP) domain decomposition method as the parallel solver is presented. More recently, a robust spectral coarse space for Schwarz domain decomposition methods based on the ACMS discretization has been introduced in [36]; further related works on CMS and ACMS methods include [12, 13, 49]. Moreover, to the authors' best knowledge, preliminary but unpublished work on the extension of the ACMS method to wave problems has been carried out by Hetmaniuk and Johnson in the early 2010s.

As a multiscale discretization, the ACMS method seems to be well suited for approximating heterogeneous Helmholtz problems. As we will discuss in this work, since the eigenmodes of the Helmholtz and the Laplacian operator are the same if the wavenumber is constant, similar ACMS basis functions as in the Laplace case are suitable for the Helmholtz equation as well.

1.2. Our contribution and outline. In this paper, we extend the ACMS method to heterogeneous Helmholtz problems. In doing so, we slightly modify the construction of the edge modes and the extension operator. These modifications are required because the weak formulation of the considered Helmholtz problem does not lead to a symmetric positive definite formulation, contrary to the elliptic case, for which the ACMS method has been developed originally. At the same time, we adapt the method to Robin boundary conditions (1.2). Moreover, edge basis functions are constructed by solving one-dimensional eigenvalue problems that are fully localized to single edges, while the edge eigenvalue problems in [41, 40, 35] solve eigenproblems that involve extensions to adjacent subdomains.

In contrast to [18, 40], where the number of subdomains in the domain decomposition is increased to obtain convergence, we perform a complementary error analysis focusing on fixing the domain decomposition and increasing the number of eigenmodes for tackling the local heterogeneities. This approach is motivated by applications from wave propagation in (quasi)-periodic media [44], where our construction yields an accurate local model for the propagation of light within one unit cell, i.e., one subdomain in the domain decomposition. While the error analysis for the local sub-problems, for which we obtain similar a posteriori error bounds as in [40] is rather simple, the error analysis for the interface problem is slightly more sophisticated. The analysis is based on the abstract framework of [32], and relies in particular on the smallness of the so-called adjoint approximability constant; see section 4 and, in particular, (4.10) below. In contrast to [32], where $H^2(\Omega)$ -regularity of the solution of the adjoint problem is required, we require H^2 -regularity of the solution of the adjoint problem only in the vicinity of the interface of the domain decomposition. We show that, upon using sufficiently many (edge) eigenmodes, the adjoint approximability constant can be made arbitrarily small, and we provide an explicit scaling relation for the required number of edge modes in terms of frequency ω .

Finally, we present a detailed numerical study of the method using a flexible implementation that, unlike in the numerical results for the ACMS method shown in previous works, also allows for unstructured meshes and domain decompositions.

The paper is organized as follows: we introduce the necessary preliminaries for defining and analyzing the ACMS method for Helmholtz problems in section 2. In particular, we show the variational formulation of the Helmholtz equation, recall the well-posedness results of [32], and illustrate the underlying domain decomposition and function spaces of the ACMS discretization. Then, in section 3, we present our new variant of the ACMS method for Helmholtz problems along with some theoretical properties. The error analysis of the ACMS method is carried out in section 4. Finally, we describe our numerical results in section 5 and conclude with some final remarks.

2. Preliminaries. In the following, we introduce the functional analytic setting and recall well-posedness results for the heterogeneous Helmholtz equation. Furthermore, we introduce the domain decomposition used in the ACMS method.

2.1. Variational formulation of the Helmholtz equation. We denote by $L^2(\Omega)$ the Lebesgue space of square-integrable functions $v : \Omega \rightarrow \mathbb{C}$ with inner product

$$(u, v)_\Omega = \int_\Omega u \bar{v} \, dx,$$

and by $H^1(\Omega)$ the usual Sobolev space of functions in $L^2(\Omega)$ with square-integrable weak derivatives. Corresponding notation is used for other measurable sets besides Ω . Furthermore, we indicate by $H_D^1(\Omega) \subset H^1(\Omega)$ functions with vanishing trace on $\Gamma_D \subset \partial\Omega$. Let us introduce the sesquilinear forms $\mathcal{A}, \mathcal{C} : H_D^1(\Omega) \times H_D^1(\Omega) \rightarrow \mathbb{C}$ defined by

$$(2.1) \quad \mathcal{A}(u, v) = \int_\Omega a \nabla u \cdot \nabla \bar{v} \, dx,$$

$$(2.2) \quad \mathcal{C}(u, v) = \mathcal{A}(u, v) - (\kappa^2 u, v)_\Omega - i(\omega \beta u, v)_{\Gamma_R}.$$

Then the weak form of the Helmholtz problem (1.1)–(1.3) and its adjoint are

$$(2.3) \quad \text{Find } u \in H_D^1(\Omega) : \quad \mathcal{C}(u, v) = F(v), \quad \text{for all } v \in H_D^1(\Omega),$$

$$(2.4) \quad \text{Find } z \in H_D^1(\Omega) : \quad \mathcal{C}(v, z) = G(v), \quad \text{for all } v \in H_D^1(\Omega).$$

Here, $F : H_D^1(\Omega) \rightarrow \mathbb{C}$ and $G : H_D^1(\Omega) \rightarrow \mathbb{C}$, defined by

$$(2.5) \quad F(v) = (f, v)_\Omega + (g, v)_{\Gamma_R},$$

$$(2.6) \quad G(v) = (v, f)_\Omega + (v, g)_{\Gamma_R},$$

are antilinear and linear functionals on $H_D^1(\Omega)$, respectively.

2.2. Well-posedness of the Helmholtz equation. We recall the well-posedness theory for the Helmholtz equation presented in [32]. Thus, we deem the following assumptions valid throughout the paper without explicitly mentioning it.

Assumption 2.1. (i) $\Omega \subset \mathbb{R}^2$ is a connected polygonal domain with piecewise C^2 boundary with strictly convex angles. Its boundary can be decomposed as $\partial\Omega = \overline{\Gamma_R} \cup \overline{\Gamma_D}$ into relatively open disjoint subsets $\Gamma_R, \Gamma_D \subset \partial\Omega$. The angle between a segment in Γ_D and Γ_R is not $\pi/2$.

(ii) The source terms satisfy $f \in L^2(\Omega)$ and $g \in H^{1/2}(\Gamma_R)$.

(iii) The coefficient functions $a, c \in L^\infty(\Omega)$ are uniformly positive, i.e., $a_{\min} \leq a(x) \leq a_{\max}$ and $c_{\min} \leq c(x) \leq c_{\max}$ for a.e. $x \in \Omega$, where $a_{\min}, c_{\min}, a_{\max}, c_{\max}$ are positive constants.

(iv) $\beta \in L^\infty(\Gamma_R)$ with $\text{meas}(\text{supp}(\beta)) > 0$ and either $\beta > 0$ or $\beta < 0$.

The analysis employs the norm $\|u\|_{\mathcal{B}}^2 = \mathcal{B}(u, u)$ induced by the sesquilinear form

$$(2.7) \quad \mathcal{B}(u, v) = \mathcal{A}(u, v) + (\kappa^2 u, v)_\Omega,$$

defined for $u, v \in H_D^1(\Omega)$. In [32, Thm. 2.4], the following result is proved. We recall parts of the proof to show robustness of the constant C_C for high-frequencies $\omega \rightarrow \infty$.

THEOREM 2.2. (i) For all $u, v \in H_D^1(\Omega)$, it holds that

$$(2.8) \quad |\mathcal{C}(u, v)| \leq C_C \|u\|_{\mathcal{B}} \|v\|_{\mathcal{B}},$$

with constant $C_C = 1 + C_\Omega \beta_{\max} \max\{a_{\min}^{-1}, \frac{1+\omega}{\omega} c_{\max}\}$ and constant C_Ω depending only on Ω .

(ii) There exist unique solutions of (2.3) and (2.4).

(iii) If $g = 0$ in (2.3) and (2.4), then there exists a constant $C_{\text{stab}} = C_{\text{stab}}(a, c, \omega, \Omega)$ such that the corresponding solutions u and z satisfy:

$$(2.9) \quad \|u\|_{\mathcal{B}} \leq C_{\text{stab}} \|f\|_{L^2(\Omega)}, \quad \|z\|_{\mathcal{B}} \leq C_{\text{stab}} \|f\|_{L^2(\Omega)}.$$

Proof. We only derive the constant C_C , for the other statements see [32, Thm. 2.4]. An application of the Cauchy-Schwarz inequality to (2.2) yields that

$$|\mathcal{C}(u, v)| \leq \|u\|_{\mathcal{B}} \|v\|_{\mathcal{B}} + (\omega|\beta|u, u)_{\Gamma_R}^{1/2} (\omega|\beta|v, v)_{\Gamma_R}^{1/2}.$$

The trace inequality yields a constant $C_\Omega > 0$ depending on Ω such that [33, p. 41]

$$\begin{aligned} (\omega|\beta|u, u)_{\Gamma_R} &\leq C_\Omega \beta_{\max} \left(\omega \|u\|_{L^2(\Omega)} \|\nabla u\|_{L^2(\Omega)} + \omega \|u\|_{L^2(\Omega)}^2 \right) \\ &\leq C_\Omega \beta_{\max} \left(\frac{c_{\max}}{\sqrt{a_{\min}}} \left\| \frac{\omega}{c} u \right\|_{L^2(\Omega)} \|\sqrt{a} \nabla u\|_{L^2(\Omega)} + \frac{c_{\max}^2}{\omega} \left\| \frac{\omega}{c} u \right\|_{L^2(\Omega)}^2 \right) \\ &\leq C_\Omega \beta_{\max} \max\left\{ \frac{1}{a_{\min}}, \frac{1+\omega}{\omega} c_{\max}^2 \right\} \|u\|_{\mathcal{B}}^2, \end{aligned}$$

from which (2.8) follows. \square

Given [Assumption 2.1](#), it follows that the solution u of (2.3) satisfies $\nabla u \in L^p(\Omega)$ for some $p > 2$ [34]. By invoking the Sobolev embedding theorem [3, p. 97], we thus have that u is Hölder continuous in $\bar{\Omega}$ with exponent $1 - 2/p$. Condition (i) in [Assumption 2.1](#) is used in [Subsection 4.4](#) below to verify higher regularity of the solution of the dual problem, see [56] for a counterexample if (i) is not satisfied.

2.3. Decomposition of the computational domain. Let $\{\Omega_j\}_{j=1}^J$ denote a conforming decomposition of Ω into J non-overlapping domains Ω_j with piecewise smooth boundaries. Furthermore, let

$$\Gamma = \bigcup_{j=1}^J \partial\Omega_j \setminus \Gamma_D$$

denote the domain decomposition interface and \mathcal{E} the set of all edges of the domain decomposition, where each edge e is an open set with either $\bar{e} = \partial\Omega_i \cap \partial\Omega_j$ for some $i \neq j$ or $e \subset \Gamma_R \cap \partial\Omega_i$ for some i . Furthermore, let $\mathcal{V} = \{p \in \Gamma\} = \Gamma \setminus \bigcup_{e \in \mathcal{E}} e$ be the set of points connecting adjacent edges, which we also refer to as the vertices of the domain decomposition.

2.4. Function spaces. The Lions–Magenes space $H_{00}^{1/2}(e)$ is defined as an interpolation space between $L^2(e)$ and $H_0^1(e)$ [46, Ch. 1, Thm. 11.7]. Therefore, it holds that $H_0^1(e) \subset H_{00}^{1/2}(e)$ densely [46, p. 10]. We have the following interpolation inequality

$$(2.10) \quad \|\eta\|_{H_{00}^{1/2}(e)} \leq C \|\eta\|_{L^2(e)}^{1/2} \|\eta\|_{H_0^1(e)}^{1/2}$$

for all $\eta \in H_0^1(e)$ [46, Proposition 23, p. 19]. The space $H^{1/2}(e)$ is defined as the interpolation space between $H^1(e)$ and $L^2(e)$; see [46, Ch. 1, Thm. 9.6.]. In view of [46, Ch. 1, Thm. 11.7], if $e \subset \partial\Omega_j$ for some $1 \leq j \leq J$, functions in $H_{00}^{1/2}(e)$ can be extended continuously by zero to functions in $H^{1/2}(\partial\Omega_j)$. Here, $H^{1/2}(\partial\Omega_j)$ denotes the space of traces of functions in $H^1(\Omega_j)$; cf. [46, Ch. 1, Thm. 8.3]. Lastly, by $H^{1/2}(\Gamma)$ we denote the space of traces on Γ , i.e., $v \in H^{1/2}(\Gamma)$ if, for all $1 \leq j \leq J$, there exist $u_j \in H^1(\Omega_j)$ such that $u_j|_{\partial\Omega_j \cap \Gamma} = v|_{\partial\Omega_j}$.

3. ACMS method. The ACMS method introduced in [41] relies on an orthogonal splitting of $H^1(\Omega)$ into interface functions $H^{1/2}(\Gamma)$ and local functions $H_0^1(\Omega_j)$, $j = 1, \dots, J$, and on the availability of basis functions with local support; while functions in $H_0^1(\Omega_j)$ generally have local support, interface basis functions with local support are constructed based on the edges and vertices that form Γ . In [41], orthogonality is characterized by the bilinear form associated to the elliptic problem. The basic idea of our extension of the ACMS method to Helmholtz problems is similar, but ‘orthogonality’ is measured with respect to the sesquilinear form \mathcal{C} defined in (2.2), which is not an inner product in general. Below we will construct spaces

$$(3.1) \quad V_S := V_{B,S_B} \oplus V_{\Gamma,S_\Gamma}$$

that are either associated to the subdomains Ω_j or to the interface Γ . In particular, the corresponding basis functions have local support and can be built locally. We now discuss the construction of the bubble space V_{B,S_B} and the interface space V_{Γ,S_Γ} in detail.

3.1. Bubble space. Let us define the local sesquilinear form $\mathcal{A}_j : H^1(\Omega_j) \times H^1(\Omega_j) \rightarrow \mathbb{C}$ as in (2.1) but with domain of integration Ω_j instead of Ω . Since \mathcal{A}_j is Hermitian, we can consider the eigenproblems: for $j = 1, \dots, J$ and $i \in \mathbb{N}$, find $(b_i^j, \lambda_i^j) \in H_0^1(\Omega_j) \times \mathbb{R}$ such that

$$(3.2) \quad \mathcal{A}_j(b_i^j, v) = \lambda_i^j (\kappa^2 b_i^j, v)_{\Omega_j} \quad \text{for all } v \in H_0^1(\Omega_j).$$

Standard theory ensures that the eigenfunctions $\{b_i^j\}_i$ form an orthogonal basis for $H_0^1(\Omega_j)$ with respect to \mathcal{A}_j and an orthonormal basis for $L^2(\Omega_j)$ with weighted inner product $(\kappa^2 u, v)_{\Omega_j}$, and that $\lambda_i^j > 0$. Furthermore, we may assume that the eigenvalues λ_i^j are ordered non-decreasingly, i.e., $\lambda_i^j \leq \lambda_l^j$ for $i \leq l$. By definition $\kappa(x) = \omega/c(x)$, and, hence, the numbers $\lambda_i^j \omega^2$ are eigenvalues of a corresponding eigenproblem that is independent of ω . As such, $\lambda_i^j \omega^2$ is independent of ω . If $c(x)$ is constant, the bubble functions are defined as in the elliptic case [41]. In slight abuse of notation, we may denote by $b_i^j \in H_0^1(\Omega)$ also the extension of $b_i^j \in H_0^1(\Omega_j)$ by zero outside of Ω_j and we call these *bubble functions*. Associated to the partition $\{\Omega_j\}_j$ of Ω , let us introduce the infinite-dimensional bubble space

$$(3.3) \quad V_B = \bigoplus_{j=1}^J V^j, \quad \text{with } V^j = \text{span}\{b_i^j : i \in \mathbb{N}\}.$$

Let $S_B = (I_1, \dots, I_J) \in \mathbb{N}^J$ be a multi-index. Then, the finite-dimensional bubble space employed in the ACMS method is defined by

$$(3.4) \quad V_{B, S_B} = \bigoplus_{j=1}^J V_{I_j}^j, \quad \text{with } V_{I_j}^j = \text{span}\{b_i^j : 1 \leq i \leq I_j\}.$$

3.2. Solvability of local Helmholtz problems. The interface space V_{Γ, S_Γ} introduced below relies on the proper extension of functions defined on the interface Γ . The extension relies on the solvability of local Helmholtz problems with homogeneous Dirichlet boundary conditions. Therefore, in the rest of the manuscript, we additionally assume the following:

Assumption 3.1. For all $j = 1, \dots, J$ and for all $i \in \mathbb{N}$, let $\lambda_i^j \neq 1$.

Assumption 3.1 might be justified by suitably adapting the partition $\{\Omega_j\}_j$ such that the spectrum of the corresponding differential operator in (4.2) does not include the value 1: the eigenvalues λ_i^j depend on the size of Ω_j , and they grow if Ω_j is suitably made smaller, cf. (3.10) for the corresponding scaling behavior of eigenvalues for one-dimensional eigenvalue problems. As noted in Subsection 3.1, the numbers $\lambda_i^j \omega^2$ are independent of ω . Hence, the suitable adjustment of $\{\Omega_j\}$ that guarantees that **Assumption 3.1** holds, depends on the frequency ω . Similar assumptions have been used, e.g., in [27, Assumption 4.2] or [18, Assumption 1], to guarantee coercivity of the local Helmholtz problems. Next, we establish well-posedness of the local Helmholtz problems under the conditions of **Assumption 3.1**.

LEMMA 3.2. For $\beta^j = \inf_{i \in \mathbb{N}} \{|\lambda_i^j - 1|/(\lambda_i^j + 1)\} > 0$, the following estimates hold:

$$\begin{aligned} \inf_{u \in H_0^1(\Omega_j)} \sup_{v \in H_0^1(\Omega_j)} \frac{\mathcal{A}_j(u, v) - (\kappa^2 u, v)_{\Omega_j}}{\|u\|_{\mathcal{B}} \|v\|_{\mathcal{B}}} &\geq \beta^j, \\ \inf_{v \in H_0^1(\Omega_j)} \sup_{u \in H_0^1(\Omega_j)} \frac{\mathcal{A}_j(u, v) - (\kappa^2 u, v)_{\Omega_j}}{\|u\|_{\mathcal{B}} \|v\|_{\mathcal{B}}} &\geq \beta^j. \end{aligned}$$

Proof. **Assumption 3.1** implies that $\beta^j > 0$. Let $u \in H_0^1(\Omega_j)$ be given. Since $\{b_i^j\}_i$ is a basis of $H_0^1(\Omega_j)$, we have that $u = \sum_{i=1}^\infty u_i b_i^j$ with $u_i = (\kappa^2 u, b_i^j)_{\Omega_j}$. Now, let $v = \sum_{i=1}^\infty \text{sgn}(\lambda_i^j - 1) u_i b_i^j$. We note that

$$\|u\|_{\mathcal{B}}^2 = \sum_{i=1}^\infty (\lambda_i^j + 1) |u_i|^2,$$

and $\|v\|_{\mathcal{B}} = \|u\|_{\mathcal{B}}$. Then we have that

$$\mathcal{A}_j(u, v) - (\kappa^2 u, v)_{\Omega_j} = \sum_{i=1}^\infty |\lambda_i^j - 1| u_i^2 \geq \inf_{i \in \mathbb{N}} \frac{|\lambda_i^j - 1|}{\lambda_i^j + 1} \|u\|_{\mathcal{B}}^2.$$

Hence, the first inequality follows. The second inequality follows similarly. \square

3.3. A harmonic extension operator. In order to define the interface space, we need an extension from Γ to Ω , which is obtained by combining the extensions of functions from $\partial\Omega_j$ to Ω_j .

For a given $\tau \in H^{1/2}(\partial\Omega_j)$, let $\tilde{\tau} \in H^1(\Omega_j)$ be any function satisfying $\tilde{\tau}|_{\partial\Omega_j} = \tau$. Then, we indicate by $\tilde{\tau}_0 \in H_0^1(\Omega_j)$ the solution to

$$(3.5) \quad \mathcal{A}_j(\tilde{\tau}_0, v) - (\kappa^2 \tilde{\tau}_0, v)_{\Omega_j} = -(\mathcal{A}_j(\tilde{\tau}, v) - (\kappa^2 \tilde{\tau}, v)_{\Omega_j}) \quad \text{for all } v \in H_0^1(\Omega_j),$$

which is uniquely defined by **Lemma 3.2**. We introduce the local Helmholtz-harmonic extension $E^j : H^{1/2}(\partial\Omega_j) \rightarrow H^1(\Omega_j)$ by setting $E^j \tau = \tilde{\tau} + \tilde{\tau}_0$.

LEMMA 3.3. *The extension operator $E^j : H^{1/2}(\partial\Omega_j) \rightarrow H^1(\Omega_j)$ is bounded, that is,*

$$(3.6) \quad \|E^j \tau\|_{\mathcal{B}} \leq (1 + 1/\beta^j) \|\tilde{\tau}\|_{\mathcal{B}},$$

where $\tilde{\tau} \in H^1(\Omega_j)$ is any extension of $\tau \in H^{1/2}(\partial\Omega_j)$.

Proof. We estimate the right-hand side in (3.5) by $\|\tilde{\tau}\|_{\mathcal{B}} \|v\|_{\mathcal{B}}$. Then, **Lemma 3.2** yields that $\|\tilde{\tau}_0\|_{\mathcal{B}} \leq \|\tilde{\tau}\|_{\mathcal{B}}/\beta^j$, and the assertion follows. \square

We note the following orthogonality relation, which is a crucial property for the construction of the ACMS spaces: for $\tau \in H^{1/2}(\partial\Omega_j)$ and for all bubble functions $b_i^j \in H_0^1(\Omega_j)$, we have

$$(3.7) \quad \mathcal{A}_j(E^j \tau, b_i^j) - (\kappa^2 E^j \tau, b_i^j)_{\Omega_j} = 0.$$

Next, we construct extensions from the local edges and the interface. We assume that $e = \partial\Omega_j \cap \partial\Omega_i \in \mathcal{E}$ is a common edge of Ω_i and Ω_j . Let $\tau \in H^{1/2}(\Gamma)$, which, by restriction, implies $\tau \in H^{1/2}(\partial\Omega_j)$ and $\tau \in H^{1/2}(\partial\Omega_i)$. Since $(E^j \tau)|_e = \tau|_e = (E^i \tau)|_e$, we can introduce the extension operator $E^\Gamma : H^{1/2}(\Gamma) \rightarrow H_D^1(\Omega)$ by $(E^\Gamma \tau)|_{\Omega_j} = E^j \tau|_{\partial\Omega_j}$, for all $j = 1, \dots, J$. Moreover, we define $E^e : H_{00}^{1/2}(e) \rightarrow H_D^1(\Omega)$ via $E^e \tau = E^\Gamma E_0^e \tau$, where $E_0^e : H_{00}^{1/2}(e) \rightarrow H^{1/2}(\Gamma)$ denotes the extension by zero to the interface Γ .

3.4. Vertex based approximation space. For any $p \in \mathcal{V}$, let $\varphi_p : \Gamma \rightarrow \mathbb{R}$ denote a piecewise harmonic function, that is, $\Delta_e \varphi_p|_e = 0$ for all $e \in \mathcal{E}$, with Δ_e indicating the Laplace operator along the edge $e \in \mathcal{E}$, and $\varphi_p(q) = \delta_{p,q}$ for all $p, q \in \mathcal{V}$. Note that the support of φ_p consists of all edges which share the vertex p and is,

therefore, local. In turn, $E^\Gamma \varphi_p$ is supported on all subdomains Ω_j that share the vertex p . If all edges $e \in \mathcal{E}$ are straight line segments, then φ_p is a piecewise linear function on Γ , similar to [41]. The choice of Δ_e here is motivated by the error analysis in Subsection 4.3. The vertex based space is then defined by linear combinations of corresponding extensions,

$$V_{\mathcal{V}} = \text{span}\{E^\Gamma \varphi_p : p \in \mathcal{V}\}.$$

For our error analysis, we will employ the nodal interpolant

$$(3.8) \quad I_{\mathcal{V}} v = \sum_{p \in \mathcal{V}} v(p) \varphi_p,$$

which is well-defined for functions $v : \bar{\Omega} \rightarrow \mathbb{C}$ that are continuous in all $p \in \mathcal{V}$. Note that $I_{\mathcal{V}}$ can be applied to the solution $u \in H_D^1(\Omega) \cap W^{1,p}(\Omega)$ to (2.3), see the comments at the end of Subsection 2.2.

3.5. Interface space. Let us consider $e \in \mathcal{E}$ and denote by ∂_e the tangential derivative, i.e., differentiation along e . We define the edge modes as solutions to the following weak formulation of the edge-Laplace eigenvalue problems: for each $e \in \mathcal{E}$ find $(\tau_i^e, \lambda_i^e) \in H_0^1(e) \times \mathbb{R}$, $i \in \mathbb{N}$, such that

$$(3.9) \quad (\partial_e \tau_i^e, \partial_e \eta)_e = \lambda_i^e (\tau_i^e, \eta)_e \quad \text{for all } \eta \in H_0^1(e).$$

Standard theory ensures that the eigenfunctions $\{\tau_i^e\}_i$ form an orthogonal basis for $H_0^1(e)$ and an orthonormal basis for $L^2(e)$. We may again assume that the eigenvalues $\lambda_j^e > 0$ are ordered increasingly. Moreover, we note that the asymptotic behavior of the eigenvalues is [20, p. 415]

$$(3.10) \quad \lambda_i^e \sim \left(\frac{i\pi}{|e|}\right)^2.$$

Let us mention that the definition of the edge modes here involves the resolution of local problems on single edges and it differs from the definition in the classical ACMS method of [41, 40], where the authors solve eigenvalue problems involving the extension operator. The corresponding infinite-dimensional interface space is

$$(3.11) \quad V_{\Gamma} = V_{\mathcal{V}} + \sum_{e \in \mathcal{E}} E^e V^e, \quad V^e = \text{span}\{\tau_i^e : i \in \mathbb{N}\}.$$

Note that each function in $E^e V^e$ has local support inside the two subdomains adjacent to e . Choosing $I_e \in \mathbb{N}$, $e \in \mathcal{E}$, we introduce the $L^2(e)$ -projection $P_{I_e}^e : L^2(e) \rightarrow V^e$ defined by

$$(3.12) \quad P_{I_e}^e v = \sum_{j=1}^{I_e} (v, \tau_j^e)_e \tau_j^e,$$

and denote the range of $P_{I_e}^e$ by $V_{I_e}^e$. Collecting the indices I_e in a multi-index S_{Γ} , we define the finite-dimensional interface space by

$$(3.13) \quad V_{\Gamma, S_{\Gamma}} = V_{\mathcal{V}} + \sum_{e \in \mathcal{E}} E^e V_{I_e}^e,$$

which, together with (3.4), completes the construction of the ACMS approximation space in (3.1). We now give some well-known interpolation error estimates. We recall the proofs for convenience of the reader.

LEMMA 3.4. *For any $e \in \mathcal{E}$ and all $w \in H_0^1(e)$, it holds that*

$$(3.14) \quad \|w - P_{I_e}^e w\|_{L^2(e)} \leq \frac{1}{\sqrt{\lambda_{I_e+1}^e}} \|w - P_{I_e}^e w\|_{H^1(e)}.$$

If, additionally, $w \in H_0^1(e) \cap H^2(e)$, then there exists a constant $C > 0$ such that

$$(3.15) \quad \|w - P_{I_e}^e w\|_{H^1(e)} \leq \frac{C}{\sqrt{\lambda_{I_e+1}^e}} \|\Delta_e w - P_{I_e}^e \Delta_e w\|_{L^2(e)}.$$

Proof. Since $\{\tau_j^e\}_j$ form an orthonormal basis of $L^2(e)$, we have that

$$\|w - P_{I_e}^e w\|_{L^2(e)}^2 = \sum_{j \geq I_e+1} |(w, \tau_j^e)_e|^2 \leq \frac{1}{\lambda_{I_e+1}^e} \|w - P_{I_e}^e w\|_{H^1(e)}^2,$$

which proves (3.14). By (3.9) and the Poincaré inequality, we similarly have that

$$\|w - P_{I_e}^e w\|_{H^1(e)}^2 \leq C_P \sum_{j \geq I_e+1} \lambda_j^e |(w, \tau_j^e)_e|^2.$$

Using the definition of τ_j^e in (3.9) again and performing integration by parts, we obtain

$$(w, \tau_j^e)_e = \frac{1}{\lambda_j^e} (\partial_e w, \partial_e \tau_j^e)_e = -\frac{1}{\lambda_j^e} (\Delta_e w, \tau_j^e)_e,$$

where we used that $w, \tau_j^e \in H_0^1(e)$. This concludes the proof of (3.15). \square

LEMMA 3.5. *Let $e \in \mathcal{E}$. Then, there exists a constant $C > 0$ such that*

$$(3.16) \quad \inf_{v^e \in V_{I_e}^e} \|w - I_{\mathcal{V}} w - v^e\|_{H_{00}^{1/2}(e)} \leq \frac{C}{\sqrt{\lambda_{I_e+1}^e}} \|w\|_{H^{3/2}(e)}$$

for all $w \in H^{3/2}(e)$, with nodal interpolant $I_{\mathcal{V}} w$ defined in (3.8).

Proof. By continuity of the embedding $H^1(e) \hookrightarrow C^0(\bar{e})$, we have that the nodal interpolation operator $I_{\mathcal{V}}$ is bounded, i.e., $\|I_{\mathcal{V}} w\|_{H^1(e)} \leq C \|w\|_{H^1(e)}$ for all $w \in H^1(e)$. By choosing $v^e = 0$, we thus have the stability estimate

$$(3.17) \quad \inf_{v^e \in V_{I_e}^e} \|w - I_{\mathcal{V}} w - v^e\|_{H^1(e)} \leq C \|w\|_{H^1(e)} \quad \text{for all } w \in H^1(e).$$

Employing Lemma 3.4 and using that $w - I_{\mathcal{V}} w \in H_0^1(e)$, we also have that

$$\inf_{v^e \in V_{I_e}^e} \|w - I_{\mathcal{V}} w - v^e\|_{H^1(e)} \leq \frac{C}{\sqrt{\lambda_{I_e+1}^e}} \|w\|_{H^2(e)} \quad \text{for all } w \in H^2(e).$$

Therefore, we get by interpolation [46, Thm. 5.1, Thm. 9.6] that

$$(3.18) \quad \inf_{v^e \in V_{I_e}^e} \|w - I_{\mathcal{V}} w - v^e\|_{H^1(e)} \leq \frac{C}{(\lambda_{I_e+1}^e)^{1/4}} \|w\|_{H^{3/2}(e)} \quad \text{for all } w \in H^{3/2}(e).$$

Employing (3.18) and Lemma 3.4 and recalling that the best-approximation is realized via the projection $P_{I_e}^e(w - I_{\mathcal{V}} w)$, we also have that

$$(3.19) \quad \inf_{v^e \in V_{I_e}^e} \|w - I_{\mathcal{V}} w - v^e\|_{L^2(e)} \leq \frac{1}{(\lambda_{I_e+1}^e)^{3/4}} \|w\|_{H^{3/2}(e)} \quad \text{for all } w \in H^{3/2}(e).$$

Therefore, by the interpolation inequality (2.10), the relations (3.18) and (3.19) yield (3.16), which concludes the proof. \square

The next result shows that $H_D^1(\Omega)$ -functions can be approximated by bubble and interface functions. The proof of this statement is also the recipe to obtain quantitative error estimates in [Subsection 4.3](#).

LEMMA 3.6. *Let V_B and V_Γ be as in (3.3) and (3.11), respectively. Then it holds that $H_D^1(\Omega) = V_B \oplus V_\Gamma$.*

Proof. Using a density argument, it is sufficient to show that any function $v \in H_D^1(\Omega) \cap C_0^\infty(\Omega \cup \Gamma_R)$ can be approximated by functions in $V_B \oplus V_\Gamma$. First note that $(v - E^\Gamma v|_\Gamma)|_{\Omega_j} \in H_0^1(\Omega_j)$ for each $j = 1, \dots, J$. Therefore, $v - E^\Gamma v|_\Gamma \in V_B$. It remains to show that $E^\Gamma v|_\Gamma$ can be approximated by functions in the interface space V_Γ . By continuity of E^Γ , it is sufficient to approximate $v|_{\partial\Omega_j}$ in $H^{1/2}(\partial\Omega_j)$. First, we subtract the nodal interpolant, and observe that $(v - I_V v)|_e \in H_0^1(e) \subset H_{00}^{1/2}(e)$ for any $e \in \mathcal{E}$ such that $e \subset \partial\Omega_j$. Then, $\|v - I_V v\|_{H^{1/2}(\partial\Omega_j)}$ can be localized to single edges $e \subset \partial\Omega_j$ as follows: define $w^e \in H^{1/2}(\partial\Omega_j)$ via $w^e = (v - I_V v)|_e$ and $w^e = 0$ on $\partial\Omega_j \setminus e$. We observe that $v - I_V v = \sum_{e \subset \partial\Omega_j} w^e$ on $\partial\Omega_j$. From [\[33, Lemma 1.3.2.6\]](#), we have that $\|w^e\|_{H^{1/2}(\partial\Omega_j)}$ is equivalent to $\|w^e\|_{H_{00}^{1/2}(e)}$. Since it holds $\|v - I_V v\|_{H^{1/2}(\partial\Omega_j)} \leq \sum_{e \subset \partial\Omega_j} \|w^e\|_{H^{1/2}(\partial\Omega_j)} \leq C \sum_{e \subset \partial\Omega_j} \|w^e\|_{H_{00}^{1/2}(e)}$, the result follows from noting that $w|_e \in V^e$. \square

4. Galerkin approximation. We start by observing that

$$(4.1) \quad \mathcal{C}(v_B, v_\Gamma) = \mathcal{A}(v_B, v_\Gamma) - (\kappa^2 v_B, v_\Gamma) - i(\omega \beta v_B, v_\Gamma)_{\Gamma_R} = 0,$$

for all $v_B \in V_B$ and $v_\Gamma \in V_\Gamma$, where we used (3.7) and that $v_B = 0$ on Γ_R . Since $u = u_B + u_\Gamma \in V_B \oplus V_\Gamma$ with $u_B = u - E^\Gamma u|_\Gamma$ and $u_\Gamma = E^\Gamma u|_\Gamma$, we thus obtain that

$$(4.2) \quad \mathcal{C}(u_B, v_B) = F(v_B) \quad \text{for all } v_B \in V_B \quad \text{and}$$

$$(4.3) \quad \mathcal{C}(u_\Gamma, v_\Gamma) = F(v_\Gamma) \quad \text{for all } v_\Gamma \in V_\Gamma.$$

Recalling that $V_S = V_{B,S_B} \oplus V_{\Gamma,S_\Gamma}$ has been defined in (3.1), with $V_{B,S_B} \subset V_B$ and $V_{\Gamma,S_\Gamma} \subset V_\Gamma$ defined in (3.4) and (3.13), respectively, the Galerkin approximations of (4.2)–(4.3) are split into two independent problems, namely a *bubble approximation*: find $u_{B,S} \in V_{B,S_B}$ such that

$$(4.4) \quad \mathcal{C}(u_{B,S}, v_{B,S}) = F(v_{B,S}) \quad \text{for all } v_{B,S} \in V_{B,S_B};$$

and an *interface approximation*: find $u_{\Gamma,S} \in V_{\Gamma,S_\Gamma}$ such that

$$(4.5) \quad \mathcal{C}(u_{S,\Gamma}, v_{S,\Gamma}) = F(v_{S,\Gamma}) \quad \text{for all } v_{S,\Gamma} \in V_{\Gamma,S_\Gamma}.$$

The Galerkin problem (4.4) is well-posed under [Assumption 3.1](#), while adjoint approximability is required to analyze the Galerkin problem (4.5); cf. [\[32\]](#). In [Theorem 4.9](#) below, we prove estimates for the adjoint approximability constant, ensuring that also (4.5) is well-posed as long as the number of edge modes is sufficiently large. In the following subsections, we present an error analysis for the two independent approximation problems (4.4) and (4.5).

4.1. Error estimates for the bubble approximation. For the statement of the approximation result, let us introduce the L^2 -projection $P_{I_j}^j : L^2(\Omega) \rightarrow V_{I_j}^j$, given by

$$(4.6) \quad P_{I_j}^j f = \sum_{i=1}^{I_j} (\kappa^2 f, b_i^j)_{\Omega_j} b_i^j.$$

The error analysis is then straight-forward, and the proof is given for convenience of the reader.

THEOREM 4.1. *Assume $f \in L^2(\Omega)$ and set $f_\kappa := f/\kappa^2$. For $u_B \in V_B$ and $u_{B,S} \in V_{B,S_B}$, defined in (4.2) and (4.4), respectively, we have the estimates:*

$$(4.7) \quad \|\kappa(u_B - u_{B,S})\|_{L^2(\Omega)}^2 \leq \sum_{j=1}^J \frac{1}{|\lambda_*^j - 1|^2} \|\kappa(f_\kappa - P_{I_j}^j f_\kappa)\|_{L^2(\Omega_j)}^2,$$

$$(4.8) \quad \|\sqrt{a}\nabla(u_B - u_{B,S})\|_{L^2(\Omega)}^2 \leq \sum_{j=1}^J \frac{\lambda_\#^j}{|\lambda_\#^j - 1|^2} \|\kappa(f_\kappa - P_{I_j}^j f_\kappa)\|_{L^2(\Omega_j)}^2,$$

where $\lambda_*^j = \operatorname{argmin}\{|\lambda_i^j - 1|, i \geq I_j + 1\}$, and $\lambda_\#^j = \operatorname{argmax}\{\frac{\lambda_i^j}{|\lambda_i^j - 1|^2}, i \geq I_j + 1\}$.

Proof. Since $\{b_i^j\}_i$ form an orthonormal basis for $L^2(\Omega_j)$ with the weighted inner product $(\kappa^2 u, v)_{\Omega_j}$, we may assume the expansion

$$u_B = \sum_{j=1}^J \sum_{i=1}^{\infty} u_{B,i}^j b_i^j, \quad \text{with } u_{B,i}^j = (\kappa^2 u_B, b_i^j)_{\Omega_j}.$$

By testing (4.2) with $v_B = b_i^j$, for $i \in \mathbb{N}$, and observing that $\mathcal{C}(u_B, b_i^j) = \mathcal{A}_j(u_B, b_i^j) - (\kappa^2 u_B, b_i^j)_{\Omega_j}$, we infer from (3.2) that $u_{B,i}^j = F(b_i^j)/(\lambda_i^j - 1)$. Consequently, we obtain that

$$u_{B,S} = \sum_{j=1}^J \sum_{i=1}^{I_j} u_{B,S,i}^j b_i^j, \quad \text{with } u_{B,S,i}^j = F(b_i^j)/(\lambda_i^j - 1).$$

Therefore, $u_{B,S,i}^j = u_{B,i}^j$ for $1 \leq i \leq I_j$ and $1 \leq j \leq J$. Since $b_i^j = 0$ on $\partial\Omega$, we further have that $F(b_i^j) = (f, b_i^j)_\Omega$. Hence, we conclude that

$$\|\kappa(u_B - u_{B,S})\|_{L^2(\Omega)}^2 = \sum_{j=1}^J \sum_{i=I_j+1}^{\infty} \frac{1}{|\lambda_i^j - 1|^2} |(f, b_i^j)_{\Omega_j}|^2,$$

which, by (4.6) and the definition of λ_*^j , implies (4.7). Estimate (4.8) follows similarly from $\mathcal{A}_j(b_i^j, b_i^j) = \lambda_i^j$ and

$$\|\sqrt{a}\nabla(u_B - u_{B,S})\|_{L^2(\Omega)}^2 = \sum_{j=1}^J \sum_{i=I_j+1}^{\infty} \frac{\lambda_i^j}{|\lambda_i^j - 1|^2} |(f, b_i^j)_{\Omega_j}|^2. \quad \square$$

Remark 4.2. We note that, if $f|_{\Omega_j} = 0$, then $u_B|_{\Omega_j} = 0$, and the approximation error vanishes on Ω_j . Therefore, no bubble basis functions have to be computed on the corresponding domain Ω_j . If, on the other hand, f does not vanish on Ω_j , the projection error in the estimates in Theorem 4.1 might be used to adaptively choose the number of required bubble functions that guarantee a certain error bound; cf. the discussion before [40, Prop. 3.6] for the elliptic case.

Remark 4.3. From the proof of Theorem 4.1 we see that, per subdomain, the bubble approximation is a projection of the bubble part of the solution to Helmholtz equation with respect to the norms in (4.7), (4.8). Since a projection constitutes the best-approximation and Assumption 3.1 can be interpreted as a resolution condition, the bubble approximation does not suffer from the pollution effect in the sense of [9].

4.2. Well-posedness of the interface Galerkin problem. Well-posedness of the Galerkin problem and quasi-best approximation results under an adjoint approximability condition follow as in [32, Section 4], which has also been used in [18, Section 4.2] or [48, Section 3.2] in a multiscale context. To state the result let us introduce $T^*\chi = z$, mapping $\chi \in L^2(\Omega)$ to the solution $z \in H_D^1(\Omega)$ of the dual problem

$$(4.9) \quad \mathcal{C}(v, z) = (v, \chi) \quad \text{for all } v \in H_D^1(\Omega),$$

which is well-defined due to [Theorem 2.2](#). Moreover, we denote with $T_\Gamma^*\chi = E^\Gamma(z|_\Gamma) \in V_\Gamma$ the interface component of $T^*\chi$. Using (4.1), we observe that $T_\Gamma^*\chi$ is a solution to (4.9) for test functions $v \in V_\Gamma$. The approximation properties of the interface space V_{Γ, S_Γ} are measured by the adjoint approximability constant

$$(4.10) \quad \sigma^* = \sup_{\varphi \in L^2(\Omega) \setminus \{0\}} \frac{\inf_{v_{\Gamma, S} \in V_{\Gamma, S_\Gamma}} \|T_\Gamma^*(\kappa^2 \varphi) - v_{\Gamma, S}\|_{\mathcal{B}}}{\|\kappa \varphi\|}.$$

With these preparations, we can state the abstract result [32, Thm. 4.2] in our setting.

LEMMA 4.4. *Suppose that $C_C \sigma^* \leq 1/2$, where C_C is defined in (2.8) and σ^* is the adjoint approximability constant. Then, the Galerkin problem (4.5) has a unique solution, and the following estimates hold:*

$$(4.11) \quad \|u_\Gamma - u_{\Gamma, S}\|_{\mathcal{B}} \leq 2C_C \inf_{v_{\Gamma, S} \in V_{\Gamma, S_\Gamma}} \|u_\Gamma - v_{\Gamma, S}\|_{\mathcal{B}},$$

$$(4.12) \quad \|\kappa(u_\Gamma - u_{\Gamma, S})\| \leq 2C_C^2 \sigma^* \inf_{v_{\Gamma, S} \in V_{\Gamma, S_\Gamma}} \|u_\Gamma - v_{\Gamma, S}\|_{\mathcal{B}}.$$

Note that the quasi-optimality constant $2C_C$ in (4.11) is independent of ω for large ω ; see [Theorem 2.2](#). However, the result applies only if σ^* is sufficiently small, which requires sufficiently many edge modes, see [Subsection 4.4](#).

Proof. The proof follows closely [32] and is included for convenience of the reader. Denote $e_\Gamma = u_\Gamma - u_{\Gamma, S}$, and let $\psi = T_\Gamma^*(\kappa^2 e_\Gamma)$. Then, for $\psi_{\Gamma, S} \in V_{\Gamma, S_\Gamma}$ being the best-approximation of ψ in the \mathcal{B} -norm, Galerkin orthogonality yields

$$\|\kappa e_\Gamma\|^2 = \mathcal{C}(e_\Gamma, \psi) = \mathcal{C}(e_\Gamma, \psi - \psi_{\Gamma, S}) \leq C_C \sigma^* \|e_\Gamma\|_{\mathcal{B}} \|\kappa e_\Gamma\|,$$

where we used the adjoint approximability (4.10) as follows:

$$\|\psi - \psi_{\Gamma, S}\|_{\mathcal{B}} = \inf_{v_{\Gamma, S} \in V_{\Gamma, S_\Gamma}} \|T_\Gamma^*(\kappa^2 e_\Gamma) - v_{\Gamma, S}\|_{\mathcal{B}} \leq \sigma^* \|\kappa e_\Gamma\|.$$

Using Galerkin orthogonality once again, we obtain for arbitrary $v_{\Gamma, S} \in V_{\Gamma, S_\Gamma}$ that

$$\begin{aligned} \|e_\Gamma\|_{\mathcal{B}}^2 &= \Re\{\mathcal{C}(e_\Gamma, e_\Gamma)\} + 2\|\kappa^2 e_\Gamma\|^2 = \Re\{\mathcal{C}(e_\Gamma, u_\Gamma - v_{\Gamma, S})\} + 2\|\kappa^2 e_\Gamma\|^2 \\ &\leq C_C \|e_\Gamma\|_{\mathcal{B}} \|u_\Gamma - v_{\Gamma, S}\|_{\mathcal{B}} + 2(C_C \sigma^*)^2 \|e_\Gamma\|_{\mathcal{B}}^2. \end{aligned}$$

The abstract error estimates (4.11) and (4.12) then follow using the assumption $\sigma^* \leq 1/(2C_C)$. Similarly, we can prove the existence of the Galerkin projection. Assume

$$\mathcal{C}(u_{\Gamma, S}, v_{\Gamma, S}) = 0 \quad \text{for all } v_{\Gamma, S} \in V_{\Gamma, S_\Gamma}.$$

We have to show that $u_{\Gamma, S} = 0$. As before, but using the previous identity and choosing $v_{\Gamma, S}$ as the best-approximation in the \mathcal{B} -norm of $T_\Gamma^*(\kappa^2 u_{\Gamma, S})$, we obtain

$$\|\kappa u_{\Gamma, S}\|^2 = \mathcal{C}(u_{\Gamma, S}, T_\Gamma^*(\kappa^2 u_{\Gamma, S}) - v_{\Gamma, S}) \leq C_C \sigma^* \|u_{\Gamma, S}\|_{\mathcal{B}} \|\kappa u_{\Gamma, S}\|.$$

Therefore, we have that

$$\|u_{\Gamma,S}\|_{\mathcal{B}}^2 = \Re\{\mathcal{C}(u_{\Gamma,S}, u_{\Gamma,S})\} + 2\|\kappa^2 u_{\Gamma,S}\|^2 = 2\|\kappa^2 u_{\Gamma,S}\|^2 \leq 2(C_C \sigma^*)^2 \|u_{\Gamma,S}\|_{\mathcal{B}}^2,$$

which, by assumption $C_C \sigma^* \leq 1/2$, yields that $u_{\Gamma,S} = 0$. \square

4.3. Estimates of the best-approximation error in $V_{\Gamma,S}$. Quantitative estimates for the interface approximation error follow from localizing the error to single edges and applying the estimates proven in [Lemma 3.4](#).

THEOREM 4.5. *Assume that the solution u to (2.3) satisfies $u \in H^2(e)$ for all $e \in \mathcal{E}$, and denote by $u_{\Gamma,S}$ the solution to (4.5). Then,*

$$\|u_{\Gamma} - u_{\Gamma,S}\|_{\mathcal{B}} \leq \sum_{e \in \mathcal{E}} \frac{C}{(\lambda_{I_e}^e + 1)^{3/4}} \|\Delta_e u - P_{I_e}^e \Delta_e u\|_{L^2(e)}$$

for a constant $C > 0$, bounded by $O(\|\kappa\|_{\infty})$, independent of u and $u_{\Gamma,S}$.

Proof. According to [Lemma 4.4](#), it suffices to estimate the best-approximation error $\inf_{v_{\Gamma,S}} \|u_{\Gamma} - v_{\Gamma,S}\|_{\mathcal{B}}$. By continuity of u , the nodal interpolant $I_{\mathcal{V}} u$ of u is well-defined and, by construction, we obtain that $(u - I_{\mathcal{V}} u)|_e \in H_0^1(e)$. These observations motivate the choice

$$(4.13) \quad v_{\Gamma,S} = E^{\Gamma} I_{\mathcal{V}} u + \sum_{e \in \mathcal{E}} E^e P_{I_e}^e (u - I_{\mathcal{V}} u),$$

with $P_{I_e}^e$ introduced in (3.12). We then have that $u_{\Gamma}(p) - v_{\Gamma,S}(p) = 0$ for all $p \in \mathcal{V}$. Moreover, in view of [subsection 2.4](#), $(u_{\Gamma} - v_{\Gamma,S})|_e \in H_0^1(e) \subset H_{00}^{1/2}(e)$. Therefore, the error can be localized to single edges as follows

$$(4.14) \quad u_{\Gamma}|_{\Omega_j} - v_{\Gamma,S}|_{\Omega_j} = E^j (u|_{\partial\Omega_j} - v_{\Gamma,S}|_{\partial\Omega_j}) = \sum_{e \in \mathcal{E}, e \subset \partial\Omega_j} (E^e (u|_e - v_{\Gamma,S}|_e))|_{\Omega_j}.$$

From the latter identity and from the definition (2.7), we obtain the following estimate

$$(4.15) \quad \begin{aligned} \|u_{\Gamma} - v_{\Gamma,S}\|_{\mathcal{B}}^2 &\leq C \sum_j \sum_{e \in \mathcal{E}, e \subset \partial\Omega_j} \|E^e (u|_e - v_{\Gamma,S}|_e)|_{\Omega_j}\|_{\mathcal{B}}^2 \\ &\leq (a_{\max} + \|\kappa\|_{\infty}^2) C \max_j (1 + 1/\beta^j)^2 \sum_{e \in \mathcal{E}} \|u - v_{\Gamma,S}\|_{H_{00}^{1/2}(e)}^2, \end{aligned}$$

where C depends on the number of edges of a subdomain Ω_j and where we used (3.6) and equivalence of the \mathcal{B} -norm to the $H^1(\Omega_j)$ -norm. The interpolation estimate (2.10) and [Lemma 3.4](#) then yield the assertion. \square

If the solution has more regularity, the convergence improves, as long as the derivatives of the edge modes do not grow too quickly, which is true, e.g., if e is a line segment.

LEMMA 4.6. *In addition to the assumptions of [Theorem 4.5](#), suppose that $u \in H^3(e)$ for all $e \in \mathcal{E}$. Moreover, suppose that there is a constant $C > 0$ such that $|\partial_e \tau_i^e(p)| \leq C \sqrt{\lambda_i^e}$ for all $i \in \mathbb{N}$ and $p \in \partial e$. Then there is a constant $C > 0$ such that*

$$\|u_{\Gamma} - u_{\Gamma,S}\|_{\mathcal{B}} \leq C \sum_{e \in \mathcal{E}} \frac{1}{\lambda_{I_e}^e + 1} \|u\|_{H^3(e)}.$$

Proof. In view of [Theorem 4.5](#) it suffices to bound

$$\|\Delta_e u - P_{I_e}^e \Delta_e u\|_{L^2(e)} = \left(\sum_{i>I_e} |(\Delta_e u, \tau_i^e)_e|^2 \right)^{1/2}.$$

Since $-\Delta_e \tau_i^e = \lambda_i^e \tau_i^e$ on e by elliptic regularity, integration by parts yields that

$$(\Delta_e u, \tau_i^e)_e = -\frac{1}{\lambda_i^e} (\Delta_e u, \Delta_e \tau_i^e)_e = \frac{1}{\lambda_i^e} \left((\partial_e^3 u, \partial_e \tau_i^e)_e + [\Delta_e u \partial_e \tau_i^e]_q^p \right),$$

where p, q denote the endpoints of e . Therefore, using the Cauchy-Schwarz inequality, the continuity of the embedding $H^1(e) \hookrightarrow C^0(\bar{e})$ [[3](#), p. 97], we have that

$$|(\Delta_e u, \tau_i^e)_e| \leq \frac{C}{\sqrt{\lambda_i^e}} \|u\|_{H^3(e)}.$$

Then, by using [\(3.10\)](#), we have that

$$\sum_{i>I_e} |(\Delta_e u, \tau_i^e)_e|^2 \leq C \|u\|_{H^3(e)}^2 \sum_{i>I_e} \frac{1}{\lambda_i^e} \leq C \frac{\|u\|_{H^3(e)}^2}{\sqrt{\lambda_{I_e+1}^e}},$$

which proves the claim. \square

Remark 4.7. The error estimates in [Theorem 4.5](#) and [Lemma 4.6](#) assume regularity of the solution to the Helmholtz equation along the edges of the domain decomposition. By the trace theorem [[33](#)], this smoothness follows from regularity of the solution in a neighborhood of the edges, which can be established under suitable assumptions on the coefficients; see, e.g., [[30](#), Chapter 8] or [[33](#), Chapter 4] and also [Subsection 4.4](#). If the solution u enjoys less regularity than required in the above statements, corresponding error estimates can still be proven. For instance, under the regularity $u \in W^{1,p}(\Omega)$, for $p > 2$, established above, the corresponding estimate to [Theorem 4.5](#) will have the exponent $(p-2)/(4p) > 0$ instead of $3/4$. To derive the latter statement, we use that $H_0^{1-1/p}(e)$ is an interpolation space between $L^2(e)$ and $H_0^1(e)$ [[46](#), Ch. 1, Thm. 11.6], $H_{00}^{1/2}(e)$ is an interpolation space between $L^2(e)$ and $H_0^{1-1/p}(e)$ [[46](#), Ch. 1, Thm. 11.7], and that $(u - I_{\mathcal{V}} u)|_e \in W_0^{1-1/p,p}(e) \subset H_0^{1-1/p}(e) \subset H_{00}^{1/2}(e)$ can be approximated in V^e .

4.4. Estimates for adjoint approximability constant. The well-posedness and the error estimates for the interface problem in [Subsection 4.2](#) relied on the smallness of the adjoint approximability constant σ^* defined in [\(4.10\)](#). In order to estimate σ^* in our setting, we follow the ideas of [[32](#)], where they work with piecewise linear finite elements, requiring $H^2(\Omega)$ -regularity of the adjoint problem [\(4.9\)](#). Since we need to consider the interface problem only, we can require a weaker H^2 -regularity in the vicinity of the interface Γ . Let, for some fixed $\delta > 0$,

$$(4.16) \quad \Omega_\Gamma \subset \{x \in \Gamma : \text{dist}(x, \Gamma \cup \partial\Omega) < \delta\}$$

denote an open neighborhood of $\Gamma \cup \partial\Omega$ such that $\partial\Omega_\Gamma \setminus \partial\Omega$ is smooth, see [Figure 4.1](#). We start with a result similar to [Theorem 4.5](#) but with slightly weaker regularity assumptions.

LEMMA 4.8. *Let $\lambda^\Gamma = \min_e \lambda_{I_e}^e$. Then, there exists a constant $C > 0$ with $C = O(\|\kappa\|_\infty)$ such that, for all $z \in H^2(\Omega_\Gamma)$, it holds that*

$$(4.17) \quad \inf_{v_{\Gamma,S} \in V_{\Gamma,S_\Gamma}} \|E^\Gamma(z|_\Gamma) - v_{\Gamma,S}\|_{\mathcal{B}} \leq \frac{C}{\sqrt{\lambda^\Gamma}} \|z\|_{H^2(\Omega_\Gamma)}.$$

Proof. In view of (4.15), which also introduces the κ dependency of the constants, it suffices to estimate

$$\inf_{v^e \in V_{I_e}^e} \|z - I_V z - v^e\|_{H_{00}^{1/2}(e)}$$

in terms of $\|z\|_{H^2(\Omega_\Gamma)}$. By embedding, $z \in H^2(\Omega_\Gamma)$ implies that $z \in H^{3/2}(e)$ for all $e \in \mathcal{E}$, and applying Lemma 3.5 yields that

$$\inf_{v_{\Gamma,S} \in V_{\Gamma,S_\Gamma}} \|z - v_{\Gamma,S}\|_{H_{00}^{1/2}(e)} \leq \frac{C}{\sqrt{\lambda_{I_e+1}^e}} \|z\|_{H^{3/2}(e)}.$$

Hence, the definition of λ^Γ yields the assertion. \square

Assuming regularity of the coefficients of the Helmholtz problem locally around the interface Γ , we can next estimate the adjoint approximability constant.

THEOREM 4.9. *If $a \in C^{0,1}(\overline{\Omega_\Gamma})$ and $\beta \in C^{0,1}(\overline{\Gamma_R})$, then there exists a constant $C > 0$ such that $C = O(\|\kappa\|_\infty^2 C_{\text{stab}})$, with C_{stab} from (2.9), and*

$$(4.18) \quad \sigma^* \leq C/\sqrt{\lambda^\Gamma}.$$

Proof. In view of (4.10), the key for estimating σ^* is to obtain an estimate for

$$\inf_{v_{\Gamma,S} \in V_{\Gamma,S_\Gamma}} \|T_\Gamma^*(\kappa^2 \varphi) - v_{\Gamma,S}\|_{\mathcal{B}}$$

in terms of $\|\kappa \varphi\|$ for arbitrary $\varphi \in L^2(\Omega)$, where $T_\Gamma^*(\kappa^2 \varphi) \in V_\Gamma$ is the interface component of the solution to the adjoint problem (4.9). Using (4.17), we have the bound

$$\inf_{v_{\Gamma,S} \in V_{\Gamma,S_\Gamma}} \|T_\Gamma^*(\kappa^2 \varphi) - v_{\Gamma,S}\|_{\mathcal{B}} \leq \frac{C}{\sqrt{\lambda^\Gamma}} \|T^*(\kappa^2 \varphi)\|_{H^2(\Omega_\Gamma)},$$

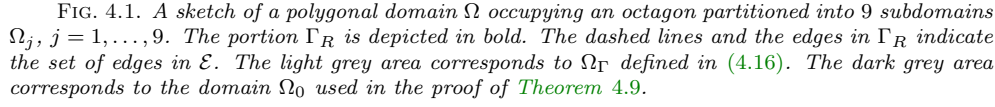
with $C = O(\|\kappa\|_\infty)$, provided $T^*(\kappa^2 \varphi) \in H^2(\Omega_\Gamma)$. Next, we show that there exists a constant $C_* > 0$ such that $C_* = O(\|\kappa\|_\infty C_{\text{stab}})$, with C_{stab} from (2.9), and

$$(4.19) \quad \|T^*(\kappa^2 \varphi)\|_{H^2(\Omega_\Gamma)} \leq C_* \|\kappa \varphi\|_{L^2(\Omega)},$$

which will conclude the proof. Let $z = T^*(\kappa^2 \varphi)$ denote the solution of the dual problem with $G(v) = (v, \kappa^2 \varphi)$, $v \in H_D^1(\Omega)$. Similar to the comments at the end of Subsection 2.2, we deduce that $z \in C^0(\overline{\Omega})$. For any $\Omega' \Subset \Omega$, [30, Theorem 8.8] ensures that

$$(4.20) \quad \|z\|_{H^2(\Omega_\Gamma \cap \Omega')} \leq C \|\kappa\|_\infty (\|z\|_{\mathcal{B}} + \|\kappa \varphi\|_{L^2(\Omega)}),$$

with a constant C depending on a_{\min} , $\|a\|_{C^{0,1}}$, and the distance of $\Omega_\Gamma \cap \Omega'$ to $\partial\Omega$ but independent of κ . Rewriting the dual problem into a Poisson problem with mixed Dirichlet-Neumann boundary conditions and applying [33, Corollary 4.4.3.8], we deduce H^2 -regularity of z also in a neighborhood of $\Gamma_R \cap \overline{\Omega_\Gamma}$ as follows. Consider



Note that, if $\Gamma_D \neq \emptyset$, then z is H^2 -regular in a neighborhood of $\partial\Omega_0 \setminus \partial\Omega$ satisfying a bound corresponding to (4.20); cf. [30, Theorem 8.12]. We observe that z is the weak solution of

with $\tilde{f} \in L^2(\Omega)$. Using [Assumption 2.1\(i\)](#) and continuity of z on $\partial\Omega_0$, we deduce that $z \in H^2(\Omega_0)$ [[33](#), Corollary 4.4.3.8]. In particular, $\partial_n z$ is in $H^{1/2}$ on each segment of $\partial\Omega_0$ [[33](#), Theorem 1.5.2.8]. Using a lifting of $\partial_n z$ as in [[28](#), Lemma 2.12], we then obtain the bound

where $\|\partial_n z\|_{H_{pw}^{1/2}(\partial\Omega_0)}$ denotes the sum of $H^{1/2}$ -norms over the corresponding segments of $\partial\Omega_0$. The $H^{1/2}(\Omega \cap \Omega_0)$ -norm of $\partial_n z$ can be bounded by the right-hand side of (4.20) using the previous considerations. The $H^{1/2}$ -norms on the segments of Γ_0 are bounded, using the boundary condition $\partial_n z = -ia^{-1}\omega\beta z$, by the corresponding $H^{1/2}$ -norms of z , which is again bounded by the terms on the right-hand side of (4.20). To bound $\|\partial_n z\|_{H^{1/2}(\Gamma_D \cap \partial\Omega_0)}$, consider $\Omega'' \Subset \Omega_0 \cup (\Gamma_D \cap \partial\Omega_0)$. An application of [30, Theorem 9.13] yields a constant $C > 0$ independent of κ such that

$$(4.22) \quad \|z\|_{H^2(\Omega'')} \leq C\|\kappa\|_\infty (\|z\|_{\mathcal{B}} + \|\kappa\varphi\|).$$

TABLE 5.1

Different errors in the L^2 - (left) and H^1 -norms (right) discussed in [section 5](#) row by row: absolute approximation errors of the ACMS solution u_S with respect to the exact solution u , absolute approximation errors of the ACMS solution u_S with respect to the finite element solution u_{FEM} , relative approximation errors of the ACMS solution u_S with respect to the finite element solution u_{FEM} , approximation errors of the finite element solution u_{FEM} with respect to the exact solution u , and interpolation error of the nodal interpolant $I_h(u)$ with respect to the exact solution u .

L^2 -errors		H^1 -errors	
e_0	$\ u - u_S\ _{L^2(\Omega)}$	e_1	$\ u - u_S\ _{H^1(\Omega)}$
$e_{0,h}$	$\ u_{\text{FEM}} - u_S\ _{L^2(\Omega)}$	$e_{1,h}$	$\ u_{\text{FEM}} - u_S\ _{H^1(\Omega)}$
$e_{0,h}^r$	$e_{0,h} / \ u_{\text{FEM}}\ _{L^2(\Omega)}$	$e_{1,h}^r$	$e_{1,h} / \ u_{\text{FEM}}\ _{H^1(\Omega)}$
$e_{0,\text{FEM}}$	$\ u - u_{\text{FEM}}\ _{L^2(\Omega)}$	$e_{1,\text{FEM}}$	$\ u - u_{\text{FEM}}\ _{H^1(\Omega)}$
$e_{0,\text{int}}$	$\ u - I_h(u)\ _{L^2(\Omega)}$	$e_{1,\text{int}}$	$\ u - I_h(u)\ _{H^1(\Omega)}$

An application of the trace theorem [[33](#), Theorem 1.5.2.8], yields a bound for $\|\partial_n z\|_{H^{1/2}(\Gamma_D \cap \partial\Omega_0)}$ in terms of the right-hand side in [\(4.22\)](#).

Combining the above estimates with [\(2.9\)](#), we infer that

$$(4.23) \quad \|z\|_{H^2(\Omega_\Gamma)} \leq C \|\kappa\|_\infty C_{\text{stab}} \|\kappa\varphi\|_{L^2(\Omega)},$$

with a constant C independent of ω . Hence [\(4.19\)](#) holds with $C_* = C \|\kappa\|_\infty C_{\text{stab}}$. \square

Since the method and its analysis presented here employ a fixed domain decomposition, the regularity assumption on the coefficients required in [Theorem 4.9](#) might be verified in certain applications; see, e.g., the periodic structure in [Subsection 5.4](#) below. A consequence of the previous result is that, by using sufficiently many edge modes, the assumptions of [Lemma 4.4](#) can be verified. More precisely, if C_{stab} is independent of ω , which holds in certain cases [[32](#), Theorem 4.5], we can use [\(3.10\)](#) and $\sigma^* = O(C_{\text{stab}} \|\kappa\|^2 \max_e |e| / \min_e I_e)$ to infer that the number of modes should scale like $I_e \geq C \|\kappa\|_\infty^2 |e|$ for stability. We obtain the following statement.

THEOREM 4.10. *In addition to the assumptions of [Theorems 4.5](#) and [4.9](#) suppose that $u \in H^{2+\alpha}(e)$ for all $e \in \mathcal{E}$, for $\alpha = 0, 1$. Then, for some $C > 0$, and λ^Γ sufficiently large, it holds*

$$\|\kappa(u_\Gamma - u_{\Gamma,S})\| \leq \frac{C}{(\lambda^\Gamma)^{5/4+\alpha/4}} \sum_{e \in \mathcal{E}} \|u\|_{H^{2+\alpha}(e)}.$$

Proof. Inserting the estimate [\(4.18\)](#) for σ^* and the error bounds stated in [Theorem 4.5](#) (if $\alpha = 0$) or [Lemma 4.6](#) (if $\alpha = 1$) into [\(4.12\)](#) yields the assertion. \square

5. Numerical results. We provide numerical experiments to support our theoretical results and show the effectiveness of our approach. Since, in general, we cannot compute the ACMS basis functions in [\(3.4\)](#) and [\(3.13\)](#) analytically, we compute them approximately using an underlying finite element discretization that adopts piecewise linear and continuous functions. To do so, we employ a quasi-uniform triangulation of the computational domain Ω into (non-curved) triangles, such that each subdomain Ω_j is the union of elements of that triangulation; see, for instance, [Figure 5.1](#). We denote the corresponding finite element solution of the Helmholtz problem by u_{FEM} . Moreover, the resulting errors are quantified according to [Table 5.1](#).

5.1. Classical Helmholtz example. Let $\Omega = B_1(0)$ be the unit disc and $\Gamma_R = \partial\Omega$. We first consider the boundary value problem given by [\(1.1\)](#) and [\(1.2\)](#) with

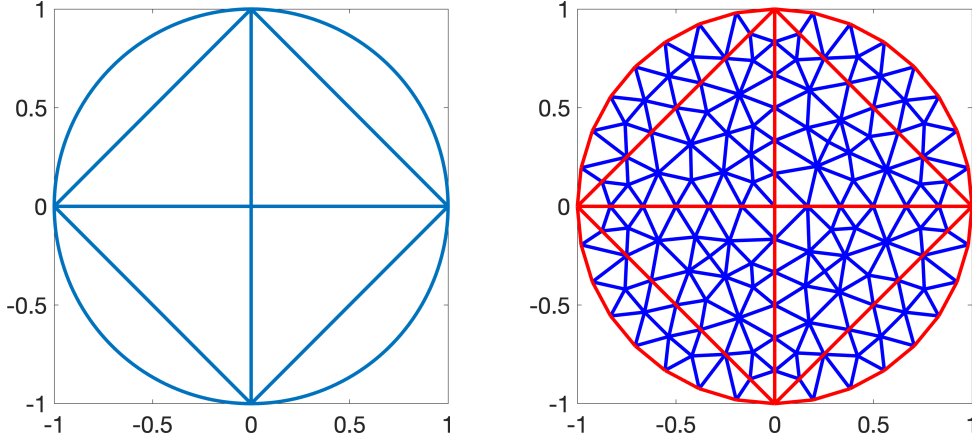


FIG. 5.1. **Left:** Ω is the unit disc, decomposed into 8 subdomains. **Right:** the corresponding coarse (red) and fine (blue) finite element meshes.

$a(x) = 1$, $\beta(x) = 1$. The source terms f and g are defined such that the problem has the plane wave solution $u(x) = \exp(-ik \cdot x)$, with wave vector $k = \kappa(0.6, 0.8)$ and variable wavenumber κ . In particular, $f(x) = 0$, therefore the solution satisfies $u_B = 0$, and u can be approximated by solving the interface problem (4.5) only; see Theorem 4.1 and also Remark 4.2.

We employ a decomposition of Ω as depicted in Figure 5.1 (left) with an initial coarse triangulation as shown in Figure 5.1 (right), which corresponds to a domain decompositions into $J = 8$ subdomains. In this domain decomposition, the number of edges in \mathcal{E} is 12 and the number of vertices in \mathcal{V} equals 5. The ACMS solution u_S and the finite element solution u_{FEM} are computed using uniform refinements of the coarse triangulation; see Figure 5.1 (right).

5.1.1. Low wavenumber. Let us first consider the case of a low wavenumber $\kappa = 1$. In this setting, we obtain $\|u\|_{H^1(\Omega)} \approx 2.5$ and $\|u\|_{L^2(\Omega)} \approx 1.8$ for the plane wave solution u . We compare the plane wave solution u with the approximation u_S given by the ACMS method for different underlying finite element discretizations and multi-indices S_Γ , which define the order of the interface approximation space V_{Γ, S_Γ} introduced in (3.13). Moreover, we use the same value of $I_e \in \{2, 4, 8, \dots, 64\}$ for each of the 12 edges in \mathcal{E} .

Table 5.2 shows the approximation error of the ACMS method and the corresponding errors for the nodal interpolant $I_h(u)$ for each mesh resolution. We observe that the H^1 -error decreases with a rate between 3.5 and 4.0, until it approaches the accuracy of the nodal interpolant $I_h u$ of the underlying finite element mesh. Similarly, the L^2 -error decays cubically for sufficiently fine finite element meshes. The L^2 -convergence is in good agreement with Theorem 4.10 and the relation $\lambda_i^e \sim i^2$ stated in (3.10), while the H^1 -convergence is better than predicted by Lemma 4.6 in this example. We may conclude that, already with a low number of edge modes $I_e \leq 32$, or which corresponds to $|S_\Gamma| \leq 384$, the ACMS solution achieves the accuracy of the nodal interpolant in the H^1 -norm, which employs around $8 \cdot 10^6$ vertices for $h \approx 3.4 \cdot 10^{-4}$. In fact, as shown in Table 5.3, the ACMS solution converges to the (standard) finite element solution u_{FEM} quadratically in the H^1 -norm and cubically in the L^2 -norm, respectively.

TABLE 5.2

Classical Helmholtz example with $\kappa = 1$: errors e_0 (top) and e_1 (bottom) as defined in Table 5.1 for different number of edge modes $|S_\Gamma| \in \{24, 28, \dots, 768\}$, computed on different finite element meshes with mesh size h , and the corresponding interpolation error for the nodal interpolant.

h	$e_{0,\text{int}}$	$ S_\Gamma $					
		24	48	96	192	384	768
$1.3 \cdot 10^{-3}$	$7.6 \cdot 10^{-7}$	$4.1 \cdot 10^{-3}$	$7.5 \cdot 10^{-4}$	$1.1 \cdot 10^{-4}$	$1.5 \cdot 10^{-5}$	$2.5 \cdot 10^{-6}$	$1.5 \cdot 10^{-6}$
$6.9 \cdot 10^{-4}$	$1.9 \cdot 10^{-7}$	$4.1 \cdot 10^{-3}$	$7.5 \cdot 10^{-4}$	$1.1 \cdot 10^{-4}$	$1.5 \cdot 10^{-5}$	$2.0 \cdot 10^{-6}$	$4.6 \cdot 10^{-7}$
$3.4 \cdot 10^{-4}$	$4.7 \cdot 10^{-8}$	$4.1 \cdot 10^{-3}$	$7.5 \cdot 10^{-4}$	$1.1 \cdot 10^{-4}$	$1.5 \cdot 10^{-5}$	$1.9 \cdot 10^{-6}$	$2.6 \cdot 10^{-7}$

h	$e_{1,\text{int}}$	$ S_\Gamma $					
		24	48	96	192	384	768
$1.3 \cdot 10^{-3}$	$1.0 \cdot 10^{-3}$	$5.7 \cdot 10^{-2}$	$1.6 \cdot 10^{-2}$	$4.3 \cdot 10^{-3}$	$1.5 \cdot 10^{-3}$	$1.1 \cdot 10^{-3}$	$1.0 \cdot 10^{-3}$
$6.9 \cdot 10^{-4}$	$5.4 \cdot 10^{-4}$	$5.7 \cdot 10^{-2}$	$1.6 \cdot 10^{-2}$	$4.2 \cdot 10^{-3}$	$1.2 \cdot 10^{-3}$	$6.0 \cdot 10^{-4}$	$5.4 \cdot 10^{-4}$
$3.4 \cdot 10^{-4}$	$2.7 \cdot 10^{-4}$	$5.7 \cdot 10^{-2}$	$1.6 \cdot 10^{-2}$	$4.2 \cdot 10^{-3}$	$1.1 \cdot 10^{-3}$	$3.8 \cdot 10^{-4}$	$2.7 \cdot 10^{-4}$

TABLE 5.3

Classical Helmholtz example with $\kappa = 1$: errors $e_{0,h}$ and $e_{1,h}$ as defined in Table 5.1 for different number of edge modes $|S_\Gamma| \in \{24, 28, \dots, 1536\}$, computed on a finite element mesh with $h \approx 3.4 \cdot 10^{-4}$ and 8327169 vertices.

	$ S_\Gamma $						
	24	48	96	192	384	768	1536
$e_{0,h}$	$4.1 \cdot 10^{-3}$	$7.5 \cdot 10^{-4}$	$1.1 \cdot 10^{-4}$	$1.5 \cdot 10^{-5}$	$1.9 \cdot 10^{-6}$	$2.5 \cdot 10^{-7}$	$3.1 \cdot 10^{-8}$
$e_{1,h}$	$5.7 \cdot 10^{-2}$	$1.6 \cdot 10^{-2}$	$4.2 \cdot 10^{-3}$	$1.0 \cdot 10^{-3}$	$2.7 \cdot 10^{-4}$	$6.9 \cdot 10^{-5}$	$1.7 \cdot 10^{-5}$

5.1.2. Higher wavenumbers. We now repeat the previous numerical experiments focusing on the effect of an increasing wavenumber; namely, we test our method for $\kappa = 2, 4, 8, 16, 32, 64, 128$. Let us mention that Assumption 3.1 is satisfied for all chosen wavenumbers and that the plane wave solution u changes with κ .

In Table 5.4, we show the convergence of the ACMS method to the plane wave solution and, for comparison, we display the error between the nodal interpolant and the finite element solution. For lower wavenumber $\kappa = 2$, we observe a similar behavior as in the previous section, i.e., close to cubic convergence of e_0 and close to quadratic convergence of e_1 until it occurs a saturation due to the limited resolution of the underlying FEM mesh.

For wavenumbers $\kappa \leq 64$, we observe that $e_{1,\text{int}}$ and $e_{1,\text{FEM}}$ behave very similarly when κ is increased. However, if $\kappa = 128$, $e_{1,\text{FEM}}$ is more than one order of magnitude larger than $e_{1,\text{int}}$, which may indicate that the FEM mesh is too coarse. For $|S_\Gamma| \geq 768$, i.e., at least 64 modes per edge, the ACMS error e_1 is close to the FEM error $e_{1,\text{FEM}}$ for all κ . We also observe that, for $\kappa \geq 32$, $|S_\Gamma|$ has to be sufficiently large to have monotonic decay in e_1 . Notably, up to a certain number of edge modes, we may even see an increase in e_1 . Ultimately, after reaching a certain threshold in the number of edge modes, which increases with κ , we observe a significant drop in the error e_1 , bringing it to a comparable level as $e_{1,\text{FEM}}$.

The convergence of the ACMS solution to the FEM solution is also verified in Table 5.5, where the corresponding errors are shown for different wavenumbers. We observe a similar convergence behavior as for e_1 and e_0 , respectively, without a saturation effect. If one is satisfied with the approximation errors achieved by u_{FEM} , we may again conclude that the ACMS method can yield good approximations already with a moderate number of degrees of freedom. We note that, by using higher order

TABLE 5.4

Classical Helmholtz example with higher wavenumbers: errors e_0 (top) and e_1 (bottom) as defined in Table 5.1 for different number of edge modes $|S_\Gamma| \in \{48, 96, \dots, 1536\}$ and wavenumbers κ , computed on a finite element mesh with $h \approx 3.4 \cdot 10^{-4}$ and 8327169 vertices. For comparison, we display the interpolation error for the nodal interpolant as well as the FEM approximation error $u_{\text{FEM}} - u$ in the H^1 - and L^2 -norm, respectively.

κ	$e_{0,\text{int}}$	$e_{0,\text{FEM}}$	$ S_\Gamma $					
			48	96	192	384	768	1536
2	$1.9 \cdot 10^{-7}$	$4.4 \cdot 10^{-7}$	$2.2 \cdot 10^{-3}$	$3.5 \cdot 10^{-4}$	$4.9 \cdot 10^{-5}$	$6.6 \cdot 10^{-6}$	$9.7 \cdot 10^{-7}$	$4.5 \cdot 10^{-7}$
4	$7.6 \cdot 10^{-7}$	$3.5 \cdot 10^{-6}$	$1.3 \cdot 10^{-2}$	$1.6 \cdot 10^{-3}$	$2.1 \cdot 10^{-4}$	$2.7 \cdot 10^{-5}$	$4.9 \cdot 10^{-6}$	$3.5 \cdot 10^{-6}$
8	$3.0 \cdot 10^{-6}$	$4.2 \cdot 10^{-5}$	$1.5 \cdot 10^{-1}$	$7.8 \cdot 10^{-3}$	$8.5 \cdot 10^{-4}$	$1.1 \cdot 10^{-4}$	$4.5 \cdot 10^{-5}$	$4.2 \cdot 10^{-5}$
16	$1.2 \cdot 10^{-5}$	$4.2 \cdot 10^{-4}$	$1.2 \cdot 10^0$	$1.6 \cdot 10^{-1}$	$6.0 \cdot 10^{-3}$	$7.2 \cdot 10^{-4}$	$4.3 \cdot 10^{-4}$	$4.2 \cdot 10^{-4}$
32	$4.8 \cdot 10^{-5}$	$4.5 \cdot 10^{-3}$	$4.9 \cdot 10^0$	$2.2 \cdot 10^0$	$3.5 \cdot 10^{-1}$	$1.0 \cdot 10^{-2}$	$4.7 \cdot 10^{-3}$	$4.5 \cdot 10^{-3}$
64	$1.9 \cdot 10^{-4}$	$1.7 \cdot 10^{-2}$	$2.4 \cdot 10^0$	$2.0 \cdot 10^0$	$2.7 \cdot 10^0$	$8.7 \cdot 10^{-2}$	$1.8 \cdot 10^{-2}$	$1.7 \cdot 10^{-2}$
128	$7.7 \cdot 10^{-4}$	$4.3 \cdot 10^{-1}$	$3.4 \cdot 10^0$	$2.0 \cdot 10^0$	$4.4 \cdot 10^0$	$9.9 \cdot 10^0$	$4.8 \cdot 10^{-1}$	$4.3 \cdot 10^{-1}$

κ	$e_{1,\text{int}}$	$e_{1,\text{FEM}}$	48	96	192	384	768	1536
2	$1.0 \cdot 10^{-3}$	$1.0 \cdot 10^{-3}$	$4.9 \cdot 10^{-2}$	$1.3 \cdot 10^{-2}$	$3.8 \cdot 10^{-3}$	$1.4 \cdot 10^{-3}$	$1.1 \cdot 10^{-3}$	$1.0 \cdot 10^{-3}$
4	$4.3 \cdot 10^{-3}$	$4.3 \cdot 10^{-3}$	$2.2 \cdot 10^{-1}$	$5.6 \cdot 10^{-2}$	$1.4 \cdot 10^{-2}$	$5.6 \cdot 10^{-3}$	$4.4 \cdot 10^{-3}$	$4.3 \cdot 10^{-3}$
8	$1.7 \cdot 10^{-2}$	$1.7 \cdot 10^{-2}$	$1.8 \cdot 10^0$	$2.3 \cdot 10^{-1}$	$5.8 \cdot 10^{-2}$	$2.2 \cdot 10^{-2}$	$1.7 \cdot 10^{-2}$	$1.7 \cdot 10^{-2}$
16	$6.9 \cdot 10^{-2}$	$6.9 \cdot 10^{-2}$	$1.9 \cdot 10^1$	$3.0 \cdot 10^0$	$2.5 \cdot 10^{-1}$	$8.9 \cdot 10^{-2}$	$7.1 \cdot 10^{-2}$	$6.9 \cdot 10^{-2}$
32	$2.7 \cdot 10^{-1}$	$3.1 \cdot 10^{-1}$	$1.5 \cdot 10^2$	$7.2 \cdot 10^1$	$1.1 \cdot 10^1$	$4.9 \cdot 10^{-1}$	$3.2 \cdot 10^{-1}$	$3.1 \cdot 10^{-1}$
64	$1.1 \cdot 10^0$	$1.5 \cdot 10^0$	$1.5 \cdot 10^2$	$1.3 \cdot 10^2$	$1.7 \cdot 10^2$	$6.1 \cdot 10^0$	$1.6 \cdot 10^0$	$1.5 \cdot 10^0$
128	$4.4 \cdot 10^0$	$5.5 \cdot 10^1$	$4.4 \cdot 10^2$	$2.5 \cdot 10^2$	$5.7 \cdot 10^2$	$1.2 \cdot 10^3$	$6.2 \cdot 10^1$	$5.5 \cdot 10^1$

elements or further mesh refinements, the accuracy of u_{FEM} may be increased; see, e.g., [51, 52]. Then, we would expect that the corresponding solution of the ACMS method would also show better accuracy in approximating the exact solution. We will investigate this in future work.

5.2. Localized interior source. In certain applications, such as in geophysics [57], the source terms of the wave propagation are localized. Therefore, let us study the behavior of the ACMS method for this type of setup. Let us consider $\Omega = B_1(0)$ with $\Gamma_R = \partial\Omega$, the coefficients $a(x) = 1$ and $\beta(x) = 1$, the non-zero source function $f(x) = \exp(-200|x - x_c|^2)$, with $x_c = (1/3, 1/3)$, $\kappa = 1$, and $g \equiv 0$. For this example, no analytical expression of the solution u is available. Thus, we only investigate the convergence of the ACMS method towards the solution of the underlying finite element method, which is justified by the discussion in the previous sections.

Table 5.6 shows the results for varying numbers of bubble functions and edge modes. In view of Theorem 4.1, we note that $u_B \approx 0$ outside the subdomain Ω_j with $x_c \in \Omega_j$. Hence, for an accurate approximation, we only need bubble functions in that subdomains Ω_j . Moreover, the linear system for the bubble component is diagonal and decoupled from the interface part. Consequently, the solution coefficient corresponding to a specific bubble basis function can be computed independently from any other ACMS basis function; cf. (4.4) and (4.5).

For this highly localized source, we observe very fast convergence to the finite element solution when $I_j \geq 32$, given a sufficiently high number of edge modes. This can be explained by inspecting the proof of Theorem 4.1: using repeatedly (3.2), integration-by-parts and that f and all its derivative are negligible on $\partial\Omega_j$, we can estimate $(f, b_i^j)_{\Omega_j}$ by arbitrary powers of λ_i^j ; see also Lemma 4.6 for similar steps. For a high number of bubble functions, a saturation effect occurs. This can be due to the

TABLE 5.5

Classical Helmholtz example with higher wavenumbers: errors $e_{0,h}$ (top) and $e_{1,h}$ (bottom) as defined in Table 5.1 for different number of edge modes $|S_\Gamma| \in \{48, 96, \dots, 1536\}$ and wavenumbers κ , computed on a finite element mesh with $h \approx 3.4 \cdot 10^{-4}$ and 8327169 vertices. For comparison, we display the interpolation error for the nodal interpolant as well as the FEM approximation error $u_{\text{FEM}} - u$ in the H^1 - and L^2 -norm, respectively.

κ	$e_{0,\text{int}}$	$e_{0,\text{FEM}}$	$ S_\Gamma $					
			48	96	192	384	768	1536
2	$1.9 \cdot 10^{-7}$	$4.4 \cdot 10^{-7}$	$2.2 \cdot 10^{-3}$	$3.5 \cdot 10^{-4}$	$4.9 \cdot 10^{-5}$	$6.6 \cdot 10^{-6}$	$8.5 \cdot 10^{-7}$	$1.0 \cdot 10^{-7}$
4	$7.6 \cdot 10^{-7}$	$3.5 \cdot 10^{-6}$	$1.3 \cdot 10^{-2}$	$1.6 \cdot 10^{-3}$	$2.1 \cdot 10^{-4}$	$2.6 \cdot 10^{-5}$	$3.3 \cdot 10^{-6}$	$4.2 \cdot 10^{-7}$
8	$3.0 \cdot 10^{-6}$	$4.2 \cdot 10^{-5}$	$1.5 \cdot 10^{-1}$	$7.8 \cdot 10^{-3}$	$8.5 \cdot 10^{-4}$	$1.0 \cdot 10^{-4}$	$1.3 \cdot 10^{-5}$	$1.6 \cdot 10^{-6}$
16	$1.2 \cdot 10^{-5}$	$4.2 \cdot 10^{-4}$	$1.2 \cdot 10^0$	$1.6 \cdot 10^{-1}$	$5.8 \cdot 10^{-3}$	$5.0 \cdot 10^{-4}$	$5.4 \cdot 10^{-5}$	$6.6 \cdot 10^{-6}$
32	$4.8 \cdot 10^{-5}$	$4.5 \cdot 10^{-3}$	$4.9 \cdot 10^0$	$2.2 \cdot 10^0$	$3.4 \cdot 10^{-1}$	$7.2 \cdot 10^{-3}$	$4.3 \cdot 10^{-4}$	$3.4 \cdot 10^{-5}$
64	$1.9 \cdot 10^{-4}$	$1.7 \cdot 10^{-2}$	$2.4 \cdot 10^0$	$2.0 \cdot 10^0$	$2.7 \cdot 10^0$	$8.0 \cdot 10^{-2}$	$2.2 \cdot 10^{-3}$	$1.5 \cdot 10^{-4}$
128	$7.7 \cdot 10^{-4}$	$4.3 \cdot 10^{-1}$	$3.5 \cdot 10^0$	$2.0 \cdot 10^0$	$4.5 \cdot 10^0$	$9.9 \cdot 10^0$	$2.4 \cdot 10^{-1}$	$4.1 \cdot 10^{-3}$

κ	$e_{1,\text{int}}$	$e_{1,\text{FEM}}$	$ S_\Gamma $					
			48	96	192	384	768	1536
2	$1.0 \cdot 10^{-3}$	$1.0 \cdot 10^{-3}$	$4.9 \cdot 10^{-2}$	$1.3 \cdot 10^{-2}$	$3.6 \cdot 10^{-3}$	$9.4 \cdot 10^{-4}$	$2.4 \cdot 10^{-4}$	$6.0 \cdot 10^{-5}$
4	$4.3 \cdot 10^{-3}$	$4.3 \cdot 10^{-3}$	$2.2 \cdot 10^{-1}$	$5.6 \cdot 10^{-2}$	$1.4 \cdot 10^{-2}$	$3.6 \cdot 10^{-3}$	$9.0 \cdot 10^{-4}$	$2.2 \cdot 10^{-4}$
8	$1.7 \cdot 10^{-2}$	$1.7 \cdot 10^{-2}$	$1.8 \cdot 10^0$	$2.3 \cdot 10^{-1}$	$5.6 \cdot 10^{-2}$	$1.4 \cdot 10^{-2}$	$3.5 \cdot 10^{-3}$	$8.9 \cdot 10^{-4}$
16	$6.9 \cdot 10^{-2}$	$6.9 \cdot 10^{-2}$	$1.9 \cdot 10^1$	$3.0 \cdot 10^0$	$2.4 \cdot 10^{-1}$	$5.5 \cdot 10^{-2}$	$1.4 \cdot 10^{-2}$	$3.5 \cdot 10^{-3}$
32	$2.7 \cdot 10^{-1}$	$3.1 \cdot 10^{-1}$	$1.5 \cdot 10^2$	$7.2 \cdot 10^1$	$1.1 \cdot 10^1$	$3.4 \cdot 10^{-1}$	$5.9 \cdot 10^{-2}$	$1.4 \cdot 10^{-2}$
64	$1.1 \cdot 10^0$	$1.5 \cdot 10^0$	$1.5 \cdot 10^2$	$1.3 \cdot 10^2$	$1.7 \cdot 10^2$	$5.6 \cdot 10^0$	$2.8 \cdot 10^{-1}$	$5.8 \cdot 10^{-2}$
128	$4.4 \cdot 10^0$	$5.5 \cdot 10^1$	$4.4 \cdot 10^2$	$2.6 \cdot 10^2$	$5.7 \cdot 10^2$	$1.2 \cdot 10^3$	$3.1 \cdot 10^1$	$5.9 \cdot 10^{-1}$

limited quantity of edge modes or to the fact that the values of higher-order derivatives of f are not negligible anymore. When increasing the number of selected edge modes while keeping the number of bubble functions fixed, the convergence approaches the predicted quadratic and cubic rates for the H^1 - and the L^2 -error, respectively. Since the Galerkin problems for the bubble part and the interface are decoupled (see (4.2) and (4.3)), the size of the systems to be solved remains comparably small. Therefore, we conclude that, for a moderate number of degrees of freedom, we obtain very good approximations of the finite element solution.

5.3. Localized boundary source. Next, let us modify the classical Helmholtz example from subsection 5.1 such that $\kappa = 16$, $f = 0$, and $g(x) = \exp(-200|x - x_c|^2)$, with $x_c = (-1/\sqrt{2}, 1/\sqrt{2})$. In Figure 5.2, we display the real and imaginary part of the finite element solution computed on a quasi-uniform mesh with 521217 vertices, i.e., $h \approx 1.3 \cdot 10^{-3}$. Although the source is very localized around x_c , the whole domain is excited, indicating the wave-type behavior of the solution.

Since $f = 0$ here, we do not need any bubble functions to obtain convergence according to Remark 4.2. As we do not have an analytic solution, we investigate the error between u_{FEM} and u_S for varying number of edge modes. The results are shown in Table 5.7, where we consider the relative errors since the solution values are rather small. As predicted by Theorem 4.5, we observe second order convergence for the H^1 -error, while the decay is initially slightly faster. The L^2 -error shows a similar behavior with a convergence rate approaching third order; cf. Theorem 4.10. We again may conclude that we can approximate the highly resolved standard finite element solution using a moderate number of edge modes in the ACMS method.

5.4. Periodic structure. Let us conclude our numerical experiments with a heterogeneous Helmholtz problem on the unit square $\Omega = [0, 1]^2$ with a domain de-

TABLE 5.6

Example 5.2 with a localized interior source. Error $e_{0,h}$ (top) and $e_{1,h}$ (bottom) as defined in Table 5.1 for different number of edge modes $|S_\Gamma| \in \{24, 28, \dots, 768\}$ (in columns) and bubble functions $|S_B|$ (in rows) for $h = 2.8 \cdot 10^{-3}$.

$ S_B $	$ S_\Gamma $						
	24	48	96	192	384	768	1536
2	$5.4 \cdot 10^{-2}$	$4.8 \cdot 10^{-2}$	$4.7 \cdot 10^{-2}$	$4.7 \cdot 10^{-2}$	$4.7 \cdot 10^{-2}$	$4.7 \cdot 10^{-2}$	$4.7 \cdot 10^{-2}$
4	$2.9 \cdot 10^{-2}$	$2.6 \cdot 10^{-2}$	$2.6 \cdot 10^{-2}$	$2.6 \cdot 10^{-2}$	$2.6 \cdot 10^{-2}$	$2.6 \cdot 10^{-2}$	$2.6 \cdot 10^{-2}$
8	$2.5 \cdot 10^{-2}$	$1.7 \cdot 10^{-2}$	$1.7 \cdot 10^{-2}$	$1.7 \cdot 10^{-2}$	$1.7 \cdot 10^{-2}$	$1.7 \cdot 10^{-2}$	$1.7 \cdot 10^{-2}$
16	$2.1 \cdot 10^{-2}$	$9.9 \cdot 10^{-3}$	$9.5 \cdot 10^{-3}$	$9.5 \cdot 10^{-3}$	$9.5 \cdot 10^{-3}$	$9.5 \cdot 10^{-3}$	$9.5 \cdot 10^{-3}$
32	$1.9 \cdot 10^{-2}$	$4.4 \cdot 10^{-3}$	$3.2 \cdot 10^{-3}$	$3.2 \cdot 10^{-3}$	$3.2 \cdot 10^{-3}$	$3.2 \cdot 10^{-3}$	$3.2 \cdot 10^{-3}$
64	$1.9 \cdot 10^{-2}$	$2.8 \cdot 10^{-3}$	$6.2 \cdot 10^{-4}$	$6.1 \cdot 10^{-4}$	$6.1 \cdot 10^{-4}$	$6.1 \cdot 10^{-4}$	$6.1 \cdot 10^{-4}$
128	$1.9 \cdot 10^{-2}$	$2.8 \cdot 10^{-3}$	$1.5 \cdot 10^{-4}$	$4.3 \cdot 10^{-5}$	$4.2 \cdot 10^{-5}$	$4.2 \cdot 10^{-5}$	$4.2 \cdot 10^{-5}$
256	$1.9 \cdot 10^{-2}$	$2.8 \cdot 10^{-3}$	$1.4 \cdot 10^{-4}$	$1.0 \cdot 10^{-5}$	$1.4 \cdot 10^{-6}$	$3.6 \cdot 10^{-7}$	$3.1 \cdot 10^{-7}$
512	$1.9 \cdot 10^{-2}$	$2.8 \cdot 10^{-3}$	$1.4 \cdot 10^{-4}$	$1.0 \cdot 10^{-5}$	$1.4 \cdot 10^{-6}$	$1.8 \cdot 10^{-7}$	$4.1 \cdot 10^{-8}$
1024	$1.9 \cdot 10^{-2}$	$2.8 \cdot 10^{-3}$	$1.4 \cdot 10^{-4}$	$1.0 \cdot 10^{-5}$	$1.4 \cdot 10^{-6}$	$1.8 \cdot 10^{-7}$	$3.1 \cdot 10^{-8}$

$ S_B $	24	48	96	192	384	768	1536
2	$3.6 \cdot 10^{-1}$	$3.4 \cdot 10^{-1}$	$3.4 \cdot 10^{-1}$	$3.4 \cdot 10^{-1}$	$3.4 \cdot 10^{-1}$	$3.4 \cdot 10^{-1}$	$3.4 \cdot 10^{-1}$
4	$2.6 \cdot 10^{-1}$	$2.4 \cdot 10^{-1}$	$2.4 \cdot 10^{-1}$	$2.4 \cdot 10^{-1}$	$2.4 \cdot 10^{-1}$	$2.4 \cdot 10^{-1}$	$2.4 \cdot 10^{-1}$
8	$2.1 \cdot 10^{-1}$	$1.9 \cdot 10^{-1}$	$1.8 \cdot 10^{-1}$	$1.8 \cdot 10^{-1}$	$1.8 \cdot 10^{-1}$	$1.8 \cdot 10^{-1}$	$1.8 \cdot 10^{-1}$
16	$1.6 \cdot 10^{-1}$	$1.2 \cdot 10^{-1}$	$1.2 \cdot 10^{-1}$	$1.2 \cdot 10^{-1}$	$1.2 \cdot 10^{-1}$	$1.2 \cdot 10^{-1}$	$1.2 \cdot 10^{-1}$
32	$1.1 \cdot 10^{-1}$	$5.9 \cdot 10^{-2}$	$5.4 \cdot 10^{-2}$	$5.4 \cdot 10^{-2}$	$5.4 \cdot 10^{-2}$	$5.4 \cdot 10^{-2}$	$5.4 \cdot 10^{-2}$
64	$1.0 \cdot 10^{-1}$	$2.7 \cdot 10^{-2}$	$1.3 \cdot 10^{-2}$	$1.3 \cdot 10^{-2}$	$1.3 \cdot 10^{-2}$	$1.3 \cdot 10^{-2}$	$1.3 \cdot 10^{-2}$
128	$1.0 \cdot 10^{-1}$	$2.3 \cdot 10^{-2}$	$2.5 \cdot 10^{-3}$	$1.2 \cdot 10^{-3}$	$1.2 \cdot 10^{-3}$	$1.2 \cdot 10^{-3}$	$1.2 \cdot 10^{-3}$
256	$1.0 \cdot 10^{-1}$	$2.3 \cdot 10^{-2}$	$2.2 \cdot 10^{-3}$	$3.6 \cdot 10^{-4}$	$9.6 \cdot 10^{-5}$	$2.8 \cdot 10^{-5}$	$1.5 \cdot 10^{-5}$
512	$1.0 \cdot 10^{-1}$	$2.3 \cdot 10^{-2}$	$2.2 \cdot 10^{-3}$	$3.6 \cdot 10^{-4}$	$9.6 \cdot 10^{-5}$	$2.5 \cdot 10^{-5}$	$8.1 \cdot 10^{-6}$
1024	$1.0 \cdot 10^{-1}$	$2.3 \cdot 10^{-2}$	$2.2 \cdot 10^{-3}$	$3.6 \cdot 10^{-4}$	$9.5 \cdot 10^{-5}$	$2.5 \cdot 10^{-5}$	$7.9 \cdot 10^{-6}$

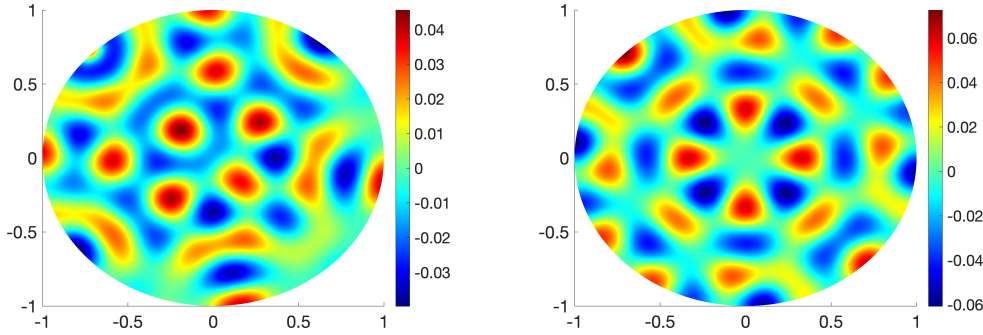


FIG. 5.2. Finite element solution of the model problem with a localized boundary source from subsection 5.3: real part (left) and imaginary part (right).

composition as in Figure 5.3 (left) and with a heterogeneous diffusion coefficient a depicted in Figure 5.3 (right). This configuration is similar to the modeling of two-dimensional photonic crystals [44]. We choose $\beta(x) = 1$, interior source $f = 0$, and the localized boundary source on $\Gamma_R = \partial\Omega$, $g(x) = \exp(-\iota k \cdot x) \exp(-100|x - x_c|^2)$, with $x_c = (0, 1/2)$, wave vector $k = \kappa(1, 0)$ and wavenumber $\kappa = 100$. The corresponding finite element solution, which has been computed on a quasi-uniform triangulation with 5 330 337 vertices, is shown in Figure 5.4.

Since, again, $f = 0$, we only need to study the behavior for varying numbers of

TABLE 5.7

Example 5.4: Localized boundary source: relative errors $e_{0,h}^r$ and $e_{1,h}^r$ as defined in Table 5.1 for different number of edge modes $|S_\Gamma| \in \{24, 28, \dots, 3072\}$, computed on a grid with $h = 1.3 \cdot 10^{-3}$.

	$ S_\Gamma $							
	24	48	96	192	384	768	1536	3072
$e_{0,h}^r$	$1.6 \cdot 10^0$	$1.0 \cdot 10^0$	$1.7 \cdot 10^{-1}$	$7.3 \cdot 10^{-3}$	$4.1 \cdot 10^{-4}$	$3.3 \cdot 10^{-5}$	$3.5 \cdot 10^{-6}$	$4.3 \cdot 10^{-7}$
$e_{1,h}^r$	$1.6 \cdot 10^0$	$1.0 \cdot 10^0$	$1.8 \cdot 10^{-1}$	$1.4 \cdot 10^{-2}$	$1.9 \cdot 10^{-3}$	$4.6 \cdot 10^{-4}$	$1.1 \cdot 10^{-4}$	$2.8 \cdot 10^{-5}$

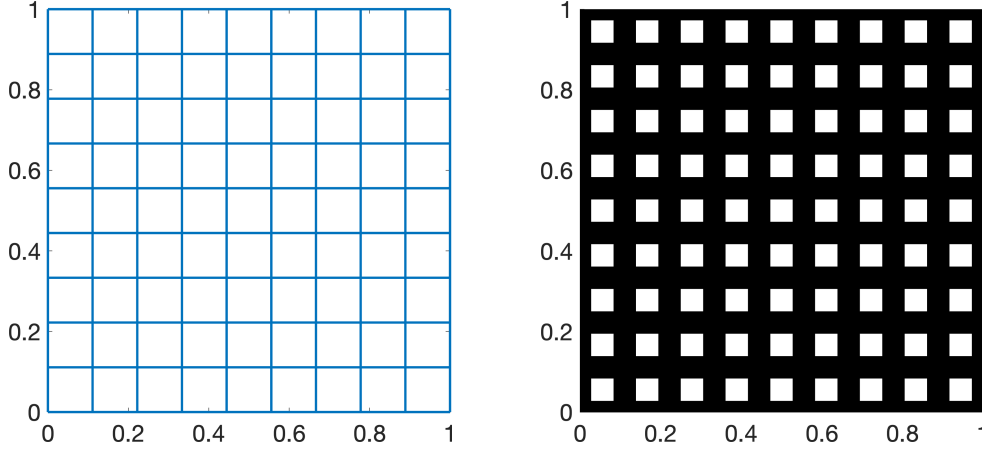


FIG. 5.3. **Left:** unit square divided in 81 subdomains for domain decomposition. The number of edges in \mathcal{E} is 180 and the number of vertices in \mathcal{V} is 100. **Right:** heterogeneous diffusion coefficient with $a = 1$ in the black regions and $a = 12$ in the white regions of the unit square.

edge modes, while the bubble part of the solution u_B is zero. Note that we can choose Ω_Γ defined in (4.16) inside the region with $a = 1$; cf. Figure 5.3. The relative H^1 - and L^2 -errors between the finite element solution and the ACMS solution are listed in Table 5.8. For $|S_\Gamma| = 2880$, which corresponds to the case of 16 modes per edge, the ACMS discretization already yields a good approximation to the highly resolved finite element solution. Moreover, the convergence of the error is initially even better than predicted by our theoretical results for $|S_\Gamma| \geq 720$.

Conclusions. We extended the ACMS method, which has originally been developed for elliptic problems, to the heterogeneous Helmholtz equation. This framework is based on a decomposition into local Helmholtz problems and an interface problem, that can be solved separately. The numerical approximation of those problems is achieved by using basis functions with local support and which can be constructed locally as well.

The error analysis developed for the investigated method is based on the abstract framework introduced in [32]. We proved error estimates in the H^1 - and the L^2 -norm, and we obtained algebraic decay in the number of basis functions (modes) being used. In order to be able to apply the framework of [32], we presented estimates for the adjoint approximability constants, showing that the number of edgemodes should scale essentially like ω^2 . Moreover, we showed applicability of the method also if the diffusion coefficient is not smooth, as long as smoothness in a neighborhood of the interface is guaranteed.

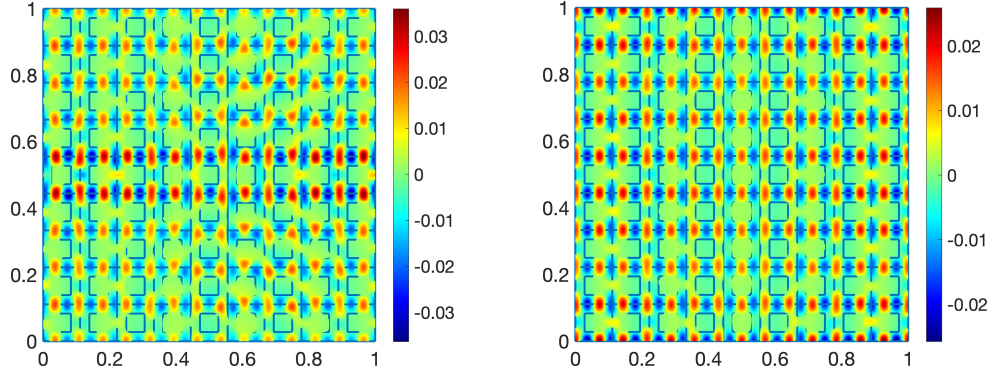


FIG. 5.4. Finite element solution of the model problem with a localized boundary source from subsection 5.4: real part (left) and imaginary part (right); the underlying structure of the coefficient a is shown as well.

TABLE 5.8

Example 5.4: Periodic structure. Relative errors $e_{0,h}^r$ and $e_{1,h}^r$ as defined in Table 5.1 for different number of edge modes $|S_\Gamma|$ computed on a grid with 5 330 337 vertices.

	$ S_\Gamma $					
	360	720	1 440	2 880	5 760	11 520
$e_{0,h}^r$	$1.1 \cdot 10^0$	$1.3 \cdot 10^0$	$1.6 \cdot 10^{-1}$	$1.0 \cdot 10^{-2}$	$7.5 \cdot 10^{-4}$	$5.0 \cdot 10^{-5}$
$e_{1,h}^r$	$1.1 \cdot 10^0$	$1.3 \cdot 10^0$	$1.6 \cdot 10^{-1}$	$1.1 \cdot 10^{-2}$	$1.3 \cdot 10^{-3}$	$2.9 \cdot 10^{-4}$

Finally, we exemplified the theoretical error bounds by numerical experiments, which show the accuracy of the inspected ACMS method for moderate wavenumbers. We constructed the ACMS basis functions using a finite element method, and we observed that the resulting discrete ACMS method approximates well the corresponding finite element solution. Thus, we may conclude that the accuracy of the discrete ACMS method depends on the accuracy of the underlying finite element method, and smaller errors might be achieved by using high-order finite elements.

Acknowledgments. EG and MS acknowledge support by the Dutch Research council (NWO) via grant OCENW.GROOT.2019.071. AH and MS acknowledge support by the 4TU.AMI SRI *Bridging Numerical Analysis and Machine Learning*.

REFERENCES

- [1] J. R. AARNES AND T. Y. HOU, *Multiscale domain decomposition methods for elliptic problems with high aspect ratios*, Acta Mathematicae Applicatae Sinica. English Series, 18 (2002), pp. 63–76, <https://doi.org/10.1007/s102550200004>.
- [2] A. ABDULLE, W. E. B. ENGQUIST, AND E. VANDEN-EIJNDEN, *The heterogeneous multiscale method*, Acta Numerica, 21 (2012), pp. 1–87, <https://doi.org/10.1017/S0962492912000025>.
- [3] R. A. ADAMS, *Sobolev Spaces*, Pure and Applied Mathematics, Academic Press, New York San Francisco London, 1975.
- [4] R. ALTMANN, P. HENNING, AND D. PETERSEIM, *Numerical homogenization beyond scale separation*, Acta Numerica, 30 (2021), pp. 1–86, <https://doi.org/10.1017/S0962492921000015>. Publisher: Cambridge University Press.
- [5] I. BABUŠKA, U. BANERJEE, AND J. E. OSBORN, *Generalized finite element methods — main ideas, results and perspective*, International Journal of Computational Methods, 01 (2004), pp. 67–103, <https://doi.org/10.1142/S0219876204000083>. Publisher: World Scientific Publishing Co.

- [6] I. BABUŠKA, G. CALOZ, AND J. E. OSBORN, *Special Finite Element Methods for a Class of Second Order Elliptic Problems with Rough Coefficients*, SIAM Journal on Numerical Analysis, 31 (1994), pp. 945–981, <https://doi.org/10.1137/0731051>.
- [7] I. BABUŠKA, F. IHLENBURG, E. T. PAIK, AND S. A. SAUTER, *A Generalized Finite Element Method for solving the Helmholtz equation in two dimensions with minimal pollution*, Computer Methods in Applied Mechanics and Engineering, 128 (1995), pp. 325–359, [https://doi.org/10.1016/0045-7825\(95\)00890-X](https://doi.org/10.1016/0045-7825(95)00890-X).
- [8] I. BABUŠKA AND J. E. OSBORN, *Generalized Finite Element Methods: Their Performance and Their Relation to Mixed Methods*, SIAM Journal on Numerical Analysis, 20 (1983), pp. 510–536, <https://doi.org/10.1137/0720034>.
- [9] I. M. BABUŠKA AND S. A. SAUTER, *Is the Pollution Effect of the FEM Avoidable for the Helmholtz Equation Considering High Wave Numbers?*, SIAM Journal on Numerical Analysis, 34 (1997), pp. 2392–2423, <https://doi.org/10.1137/S0036142994269186>.
- [10] N. BOOTLAND, V. DOLEAN, I. G. GRAHAM, C. MA, AND R. SCHEICHL, *GenEO coarse spaces for heterogeneous indefinite elliptic problems*, July 2021, <https://doi.org/10.48550/arXiv.2103.16703>. arXiv:2103.16703 [cs, math].
- [11] A. BOURGEOUS, M. BOURGET, P. LAILLY, M. POULET, P. RICARTE, AND R. VERSTEEG, *Marmousi, model and data*, in Proceedings of the 1990 EEAG Workshop on Practical Aspects of Seismic Data Inversion, R. Versteeg and G. Grau, eds., Zeist, 1991, EAEG, pp. 5–16.
- [12] F. BOURQUIN, *Analysis and comparison of several component mode synthesis methods on one-dimensional domains*, Numerische Mathematik, 58 (1990), pp. 11–33, <https://doi.org/10.1007/BF01385608>.
- [13] F. BOURQUIN, *Component mode synthesis and eigenvalues of second order operators : discretization and algorithm*, ESAIM: Mathematical Modelling and Numerical Analysis, 26 (1992), pp. 385–423, <https://doi.org/10.1051/m2an/1992260303851>.
- [14] D. L. BROWN, D. GALLISTL, AND D. PETERSEIM, *Multiscale Petrov-Galerkin method for high-frequency heterogeneous Helmholtz equations*, in Meshfree methods for partial differential equations VIII, vol. 115 of Lect. Notes Comput. Sci. Eng., Springer, Cham, 2017, pp. 85–115, https://doi.org/10.1007/978-3-319-51954-8_6.
- [15] M. BUCK, O. ILIEV, AND H. ANDRĂ, *Multiscale finite element coarse spaces for the application to linear elasticity*, Open Mathematics, 11 (2013), pp. 680–701, <https://doi.org/10.2478/s11533-012-0166-8>. Publisher: De Gruyter Open Access.
- [16] T. CHAUMONT-FRELET AND S. NICAISE, *Wavenumber explicit convergence analysis for finite element discretizations of general wave propagation problems*, IMA Journal of Numerical Analysis, 40 (2020), pp. 1503–1543, <https://doi.org/10.1093/imanum/drz020>.
- [17] Y. CHEN, T. Y. HOU, AND Y. WANG, *Exponential Convergence for Multiscale Linear Elliptic PDEs via Adaptive Edge Basis Functions*, Multiscale Modeling & Simulation, 19 (2021), pp. 980–1010, <https://doi.org/10.1137/20M1352922>.
- [18] Y. CHEN, T. Y. HOU, AND Y. WANG, *Exponentially convergent multiscale methods for 2d high frequency heterogeneous Helmholtz equations*, SIAM J. Multiscale Modeling & Simulation, 21 (2023).
- [19] L. CONEN, V. DOLEAN, R. KRAUSE, AND F. NATAF, *A coarse space for heterogeneous Helmholtz problems based on the Dirichlet-to-Neumann operator*, Journal of Computational and Applied Mathematics, 271 (2014), pp. 83–99, <https://doi.org/10.1016/j.cam.2014.03.031>.
- [20] R. COURANT AND D. HILBERT, *Methods of mathematical physics. Vol. I*, Interscience Publishers, Inc., New York, N.Y., 1953.
- [21] R. R. CRAIG AND M. C. C. BAMPION, *Coupling of substructures for dynamic analyses.*, AIAA Journal, 6 (1968), pp. 1313–1319, <https://doi.org/10.2514/3.4741>.
- [22] A. DERAEMAER, I. BABUŠKA, AND P. BOUILLARD, *Dispersion and pollution of the FEM solution for the Helmholtz equation in one, two and three dimensions*, International Journal for Numerical Methods in Engineering, 46 (1999), pp. 471–499, [https://doi.org/10.1002/\(SICI\)1097-0207\(19991010\)46:4<471::AID-NME684>3.0.CO;2-6](https://doi.org/10.1002/(SICI)1097-0207(19991010)46:4<471::AID-NME684>3.0.CO;2-6).
- [23] W. E AND B. ENGQUIST, *The heterogeneous multiscale methods*, Communications in Mathematical Sciences, 1 (2003), pp. 87–132.
- [24] Y. EFENDIEV, J. GALVIS, AND T. Y. HOU, *Generalized multiscale finite element methods (GMs-FEM)*, Journal of Computational Physics, 251 (2013), pp. 116–135, <https://doi.org/10.1016/j.jcp.2013.04.045>.
- [25] Y. EFENDIEV AND T. Y. HOU, *Multiscale Finite Element Methods*, Springer New York, New York, NY, 2009, <https://doi.org/10.1007/978-0-387-09496-0>.
- [26] Y. A. ERLANGA, C. W. OOSTERLEE, AND C. VUIK, *A novel multigrid based preconditioner for heterogeneous helmholtz problems*, SIAM Journal on Scientific Computing, 27 (2006), pp. 1471–1492, <https://doi.org/10.1137/040615195>.

- [27] P. FREESE, M. HAUCK, AND D. PETERSEIM, *Super-localized Orthogonal Decomposition for high-frequency Helmholtz problems*, arXiv: 2112.11368, (2021).
- [28] M. J. GANDER, I. G. GRAHAM, AND E. A. SPENCE, *Applying gmres to the helmholtz equation with shifted laplacian preconditioning: what is the largest shift for which wavenumber-independent convergence is guaranteed?*, *Numerische Mathematik*, 131 (2015), pp. 567–614, <https://doi.org/10.1007/s00211-015-0700-2>, <https://link.springer.com/content/pdf/10.1007/s00211-015-0700-2.pdf>.
- [29] M. J. GANDER, A. LONELAND, AND T. RAHMAN, *Analysis of a New Harmonically Enriched Multiscale Coarse Space for Domain Decomposition Methods*, Dec. 2015, <https://doi.org/10.48550/arXiv.1512.05285>. arXiv:1512.05285 [math].
- [30] D. GILBARG AND N. S. TRUDINGER, *Elliptic partial differential equations of second order*, *Classics in Mathematics*, Springer-Verlag, Berlin, 2001, <https://mathscinet-ams-org.ezproxy2.utwente.nl/mathscinet-getitem?mr=1814364>. Reprint of the 1998 edition.
- [31] S. GONG, I. G. GRAHAM, AND E. A. SPENCE, *Domain decomposition preconditioners for high-order discretisations of the heterogeneous Helmholtz equation*, Oct. 2020, <https://doi.org/10.48550/arXiv.2004.03996>. arXiv:2004.03996 [cs, math].
- [32] I. G. GRAHAM AND S. A. SAUTER, *Stability and finite element error analysis for the Helmholtz equation with variable coefficients*, *Mathematics of Computation*, 89 (2019), pp. 105–138, <https://doi.org/10.1090/mcom/3457>.
- [33] P. GRISVARD, *Elliptic Problems in Nonsmooth Domains*, Society for Industrial and Applied Mathematics, 1 2011, <https://doi.org/10.1137/1.9781611972030>.
- [34] K. GRÖGER, *A $W^{1,p}$ -estimate for solutions to mixed boundary value problems for second order elliptic differential equations*, *Math. Ann.*, 283 (1989), pp. 679–687.
- [35] A. HEINLEIN, U. HETMANIUK, A. KLAOWN, AND O. RHEINBACH, *The approximate component mode synthesis special finite element method in two dimensions: Parallel implementation and numerical results*, *Journal of Computational and Applied Mathematics*, 289 (2015), pp. 116–133, <https://doi.org/10.1016/j.cam.2015.02.053>.
- [36] A. HEINLEIN, A. KLAOWN, J. KNEPPER, AND O. RHEINBACH, *Multiscale coarse spaces for overlapping Schwarz methods based on the ACMS space in 2D*, *Electronic Transactions on Numerical Analysis*, 48 (2018), pp. 156–182, https://doi.org/10.1553/etna_vol48s156.
- [37] A. HEINLEIN, A. KLAOWN, J. KNEPPER, AND O. RHEINBACH, *Adaptive GDSW coarse spaces for overlapping Schwarz methods in three dimensions*, *SIAM Journal on Scientific Computing*, 41 (2019), pp. A3045–A3072, <https://doi.org/10.1137/18M1220613>.
- [38] A. HEINLEIN AND K. SMETANA, *A fully algebraic and robust two-level Schwarz method based on optimal local approximation spaces*, July 2022, <https://doi.org/10.48550/arXiv.2207.05559>. arXiv:2207.05559 [cs, math].
- [39] P. HENNING AND A. MÅLQVIST, *Localized orthogonal decomposition techniques for boundary value problems*, *SIAM Journal on Scientific Computing*, 36 (2014), pp. A1609–A1634.
- [40] U. HETMANIUK AND A. KLAOWN, *Error estimates for a two-dimensional special finite element method based on component mode synthesis*, *Electron. Trans. Numer. Anal.*, 41 (2014), pp. 109–132.
- [41] U. L. HETMANIUK AND R. B. LEHOUCQ, *A special finite element method based on component mode synthesis*, *ESAIM: Mathematical Modelling and Numerical Analysis*, 44 (2010), pp. 401–420, <https://doi.org/10.1051/m2an/2010007>.
- [42] T. Y. HOU AND X.-H. WU, *A Multiscale Finite Element Method for Elliptic Problems in Composite Materials and Porous Media*, *Journal of Computational Physics*, 134 (1997), pp. 169–189, <https://doi.org/10.1006/jcph.1997.5682>.
- [43] W. C. HURTY, *Vibrations of Structural Systems by Component Mode Synthesis*, *Journal of the Engineering Mechanics Division*, 86 (1960), pp. 51–69, <https://doi.org/10.1061/JMCEA3.0000162>.
- [44] J. D. JOANNOPOULOS, S. G. JOHNSON, J. N. WINN, AND R. D. MEADE, *Molding the flow of light*, Princeton Univ. Press, Princeton, NJ [ua], (2008).
- [45] D. LAFONTAINE, E. A. SPENCE, AND J. WUNSCH, *Wavenumber-explicit convergence of the hp-FEM for the full-space heterogeneous Helmholtz equation with smooth coefficients*, *Computers & Mathematics with Applications*, 113 (2022), pp. 59–69, <https://doi.org/10.1016/J.CAMWA.2022.03.007>.
- [46] J. L. LIONS AND E. MAGENES, *Non-Homogeneous Boundary Value Problems and Applications*, Springer Berlin Heidelberg, Berlin, Heidelberg, 1972, <https://doi.org/10.1007/978-3-642-65161-8>.
- [47] X. LIU, J. XIA, M. V. DE HOOP, AND X. OU, *Interconnected hierarchical structures for fast direct elliptic solution*, *Journal of Scientific Computing*, 91 (2022), p. 15, <https://doi.org/10.1007/s10915-022-01761-7>.

- [48] C. MA, C. ALBER, AND R. SCHEICHL, *Wavenumber explicit convergence of a multiscale generalized finite element method for heterogeneous Helmholtz problems*, SIAM J. Numer. Anal., 61 (2023), pp. 1546–1584.
- [49] A. MADUREIRA AND M. SARKIS, *Adaptive deluxe BDDC mixed and hybrid primal discretizations*, in Domain decomposition methods in science and engineering XXIV, vol. 125 of Lect. Notes Comput. Sci. Eng., Springer, Cham, 2018, pp. 465–473, https://doi.org/10.1007/978-3-319-93873-8_4.
- [50] A. MÅLQVIST AND D. PETERSEIM, *Localization of elliptic multiscale problems*, Mathematics of Computation, 83 (2014), pp. 2583–2603, <https://doi.org/10.1090/S0025-5718-2014-02868-8>.
- [51] J. MELENK AND S. SAUTER, *Convergence analysis for finite element discretizations of the Helmholtz equation with Dirichlet-to-Neumann boundary conditions*, Mathematics of Computation, 79 (2010), pp. 1871–1914, <https://doi.org/10.1090/S0025-5718-10-02362-8>.
- [52] J. M. MELENK AND S. SAUTER, *Wavenumber Explicit Convergence Analysis for Galerkin Discretizations of the Helmholtz Equation*, SIAM Journal on Numerical Analysis, 49 (2011), pp. 1210–1243, <https://doi.org/10.1137/090776202>.
- [53] M. OHLBERGER AND B. VERFÜRTH, *A New Heterogeneous Multiscale Method for the Helmholtz Equation with High Contrast*, Multiscale Modeling & Simulation, 16 (2018), pp. 385–411, <https://doi.org/10.1137/16M1108820>.
- [54] D. PETERSEIM, *Eliminating the pollution effect in Helmholtz problems by local subscale correction*, Mathematics of Computation, 86 (2017), pp. 1005–1036, <https://doi.org/10.1090/mcom/3156>.
- [55] D. PETERSEIM AND B. VERFÜRTH, *Computational high frequency scattering from high-contrast heterogeneous media*, Math. Comp., 89 (2020), pp. 2649–2674, <https://doi.org/10.1090/mcom/3529>.
- [56] E. SHAMIR, *Regularization of mixed second-order elliptic problems*, Israel Journal of Mathematics, 6 (1968), pp. 150–168, <https://doi.org/10.1007/BF02760180>, <https://link.springer.com/content/pdf/10.1007/BF02760180.pdf>.
- [57] S. WANG, M. V. DE HOOP, AND J. XIA, *On 3d modeling of seismic wave propagation via a structured parallel multifrontal direct helmholtz solver*, Geophysical Prospecting, 59 (2011), pp. 857–873, <https://doi.org/10.1111/j.1365-2478.2011.00982.x>.